

Ionic liquids vs conventional solvents: A comparative study in the selective catalytic oxidations promoted by oxovanadium(IV) complexes

Patrizio Campitelli^{a,b}, Massimiliano Aschi^a, Corrado Di Nicola^b, Fabio Marchetti^{b,*},
Riccardo Pettinari^c, Marcello Crucianelli^{a,*}

^a Department of Physical and Chemical Sciences, University of L'Aquila, Via Vetoio, I-67100 L'Aquila, AQ, Italy

^b School of Science and Technology, Chemistry Section, University of Camerino, Via S. Agostino 1, 62032, Camerino, MC, Italy

^c School of Pharmacy, Chemistry Section, University of Camerino, Via S. Agostino 1, 62032, Camerino, MC, Italy

ARTICLE INFO

Keywords:

Oxovanadium complexes
Olefin oxidations
Oxidative desulfurization
Acylpyrazolonate ligands
DFT calculations

ABSTRACT

Two oxovanadium(IV) complexes containing 4-acyl-5-pyrazolonate- κ^2 -O,O' bidentate ligands with different chain lengths in the acyl moiety, namely HQ^{C6} (complex I) and HQ^{C17} (complex II), have been synthesized and fully characterized, to study their catalytic activity toward the mild and selective oxidation of olefins or model organosulphur substrates, promoted by H₂O₂ or *tert*-butyl hydroperoxide (TBHP). The influence due to the type of solvent, likewise ionic liquids (ILs) or conventional medium, was analysed. H₂O₂ has proven less efficient, in comparison to TBHP. Quantum-chemical calculations have shown that, the key catalytic species involved and, consequently, the actual mechanism might be slightly different according to the oxidant used, *i.e.* the peroxy VO(Q^{Me})(O₂) adduct in the case of H₂O₂ and the *tert*-butylperoxy VO(Q^{Me})₂(OOt-Bu) adduct in the case of TBHP. Preliminary calculations suggested that, in ionic liquids, the VO(Q^{Me})₂ complex might reveal relatively unstable, hence qualitatively explaining the moderate efficiency observed in these media.

1. Introduction

The aptitude of high valent metal complexes to catalyze oxygen transfer reactions is well known from several years [1–3]. Metal complexes of Ti, V, Re, Mn or Cr are able to activate hydrogen peroxide as well as organic peroxides such as *t*-butyl- or cumyl-hydroperoxide, usually affording peroxy-, peroxy-, and oxo-type metal oxidants, thus entailing an oxygen transfer mechanism [4]. As well, the increasing interest observed in the last decades on the synthesis and reactivity of several vanadium compounds has been justified also for their involvement in biological processes [5,6] and medical applications [7], due to the dimensional and structural analogy between vanadate and phosphate ions with the possibility to mimic the phosphate group in enzymes like phosphatases and kinases. In addition, the interest toward oxovanadium containing derivatives has seen a remarkable growth also for their proven activity as oxidant promoters in oxidative catalytic reactions. In fact, oxovanadium (IV) and (V) complexes acting as oxo-transfer agents [8], are able to catalyze several oxyfunctionalization reactions such as epoxidation of alkenes [9,10], selective oxidation of organic sulphides [11], hydroxylation of phenols [12,13], oxidations of alcohols to aldehydes and ketones [14], hydro and oxidative amination [15] and oxidation of bromide [16], eventually with some degrees of

stereoselectivity, if proper chiral ligands are present in the starting complexes [17]. Often, Schiff base ligands are employed to coordinate the vanadyl (VO)²⁺ group in the oxovanadium complexes but, frequently, 4-acyl-5-pyrazolone ligands too have been investigated as versatile coordinating systems [18], also because of biological interest due to their analgesic and anti-inflammatory activity [19–21]. Mostly, catalytic oxidation with oxovanadium compounds is performed using H₂O₂ as main oxidant [22] either for olefin or sulphur oxidation [23], because it is cheap and produces only water as by-product, but several studies have been done also with *tert*-butyl hydroperoxide as oxidant [24,25], showing high conversion and very good selectivity values. The oxidation of organosulphides to their respective sulphoxides and sulphones catalysed by oxovanadium complexes has been investigated for its potential application in the oxidative desulphurization (ODS) process [26,27], also with heterogeneous polymer bound vanadium complexes [28].

Since several years, ionic liquids (ILs) have attracted rising interest with a diversified range of applications for several types of catalytic processes [29] including those promoted by oxovanadium complexes [30]. ILs present tuneable properties depending on the nature of cation or anion and their very low vapour pressure and high thermal stability make them versatile green solvents [31], with reduced environmental

* Corresponding authors.

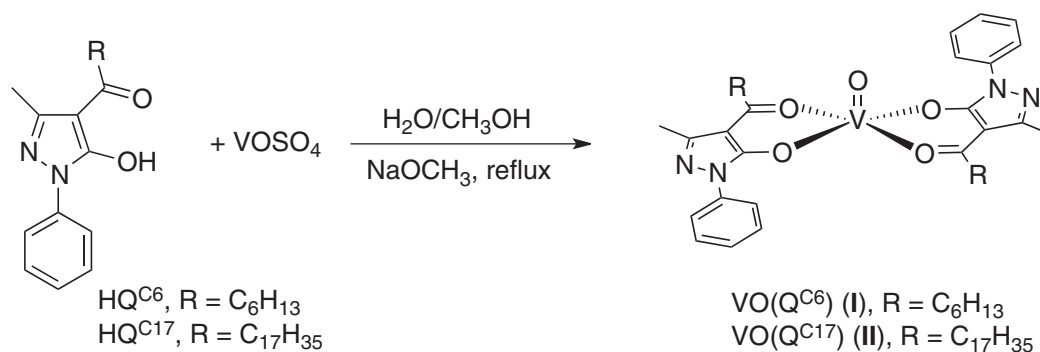
E-mail addresses: fabio.marchetti@unicam.it (F. Marchetti), marcello.crucianelli@univaq.it (M. Crucianelli).

<https://doi.org/10.1016/j.apcata.2020.117622>

Received 26 March 2020; Received in revised form 22 April 2020; Accepted 5 May 2020

Available online 08 May 2020

0926-860X/ © 2020 Elsevier B.V. All rights reserved.



Scheme 1. Synthesis of new oxovanadium complexes $\text{VO}(\text{Q}^{\text{C}6})_2$ (I) and $\text{VO}(\text{Q}^{\text{C}17})_2$ (II).

impact. An important property of ILs is their recyclability, being in theory possible to catch in their phase suitably selected organometallic complexes, thus allowing the simple recovery and reuse of precious catalysts [32]. Among others, a simple way to increase the entrapment of a metal complex, acting as a catalyst, within the IL phase is that of properly functionalize the ligands, for example with different lengths of the alkyl side-chains, thus varying the resulting hydrophobicity/hydrophilicity of the catalyst backbone, to discriminate its affinity for the chosen IL. Potentially, the role of this tag is to magnify the catalyst's partition coefficient in an appropriately selected IL. For this reason, we prepared initially two novel 4-acyl-5-pyrazolone based ligands having different chain lengths in the acyl moiety, namely $\text{HQ}^{\text{C}6}$ and $\text{HQ}^{\text{C}17}$ (containing 6 and 17 carbon atom, respectively), and then their corresponding oxovanadium(IV) complexes, i.e. $\text{VO}(\text{Q}^{\text{C}6})_2$ (I) and $\text{VO}(\text{Q}^{\text{C}17})_2$ (II), as described in the Scheme 1.

The proligand $\text{HQ}^{\text{C}17}$ has been recently used by some of us to afford Zn(II) complexes with antiproliferative activity against human breast MCF-7 cancer cells [33] and (arene)Ru(II) complexes with very potent cytotoxicity against to human ovarian A2780 carcinoma cells and the A2780cisR variant with acquired resistance to cisplatin [34], to tether the same (arene)Ru(II) complexes to polystyrene surfaces providing potent antibacterial plastics [35] and also to immobilize lanthanide complexes on the surface of pre-modified silica via hydrophobic interactions affording hybrid luminescent films [36]. Following our ongoing interest in the oxovanadium chemistry [37–39], and considering the well-established aptitude of oxovanadium(IV) complexes of promoting the activation of oxidants, especially of peroxidic nature [40], the catalytic activity of the new oxovanadium complexes (I) and (II) has been investigated in the selective oxidation of conjugated (styrene) or unconjugated (*cis*-cyclooctene) olefins and of model organosulphur derivatives as dibenzothiophene (DBT) and 4,6-dimethyldibenzothiophene (DMDBT), having in mind to compare their activity and selectivity between traditional ILs and conventional solvents. Quantum chemical DFT calculations have also been carried out to shed light on the catalytic mechanism potentially active in our experimental conditions.

2. Experimental section

2.1. Materials and methods

2.1.1. Materials

All reagents (DBT, DMDBT, styrene, *cis*-cyclooctene) and solvents were purchased from Sigma-Aldrich (Italy) in the highest purity grade available and were used as such. All ionic liquids, namely 1-butyl-3-methylimidazolium tetrafluoroborate BMIM-BF₄, 1-butyl-3-methylimidazoliumhexafluorophosphate BMIM-PF₆, 1-butyl-3-methylimidazolium trifluoromethanesulfonate BMIM-OTf, were purchased from Iolitec (<https://iolitec.de>). The $\text{HQ}^{\text{C}6}$ and $\text{HQ}^{\text{C}17}$ proligands have been synthesized according to previously reported methods [19,20,36]. Either a

70 % w/w aqueous solution (TBHP_{aq}) or a 5.5 M solution in *n*-decane of *tert*-butyl hydroperoxide (TBHP), and a 50 % w/w aqueous solution of H_2O_2 , were used as primary oxidants.

2.1.2. Analytical methods

Elemental analyses (C, H, N, S) were performed in-house with a Fisons Instruments 1108 CHNS-O Elemental Analyzer. The samples for microanalyses were dried in vacuo to constant weight (20 °C, ca. 0.1 Torr). Solid-state infrared spectra were recorded on a Perkin Elmer SpectrumOne FT-IR spectrometer. ¹H and ¹³C NMR spectra were recorded, at 25 °C, with a Bruker Avance III 400 MHz instruments. When necessary, ¹H and ¹³C NMR analyses of products were performed after flash-chromatographic purification on columns packed with silica gel (230–400 mesh), and compared with authentic sample. Microwave studies were performed with the Biotage® Initiator⁺ microwave synthesizer. The magnetic susceptibilities were measured at room temperature (20 °C) by the Gouy method, with a Sherwood Scientific Magnetic Balance MSB-Auto, using HgCo(NCS)₄ as calibrant and correcting for diamagnetism with the appropriate Pascal constants. The magnetic moments (in BM) were calculated from the equation $\mu_{\text{eff}} = 2.8428 (\chi_{\text{m}}^{\text{corr}} T)^{-1/2}$ ($\chi_{\text{m}}^{\text{corr}}$ is the molar susceptibility corrected for diamagnetism and T is the temperature in kelvin degrees). Gas chromatographic (GC) analyses were performed by means of a Hewlett-Packard 6890 series instrument equipped with a flame ionization detector (FID), using a 30 m × 0.32 mm × 0.25 μm film thickness (crosslinked 5% phenyl-methylsiloxane) column and chromatography grade helium, as carrier gas. In GC calculations, all peaks amounting to at least 0.5 % of the total products were considered. UV-vis analyses were performed with a Varian Cary 50 UV-vis Spectrophotometer, working with a thermostated UV quartz cell, at 34 °C. The 9.5 GHz Electron Paramagnetic Resonance (EPR) X-band spectrometer was a conventional assembly of Bruker units (Bruker Spectrospin, Milano, Italy) constituted by: a magnet B-M8, a resonant cavity 4108 TMH/9101, and a microwave bridge ER040XR, equipped with the field controller BH15. TGA-DTA spectra were obtained with a STA 6000 Simultaneous Thermal Analyzer Perkin-Elmer. Inductively coupled plasma atomic emission spectrometry (ICP-AES) analyses were performed using a Varian Liberty 200 spectrophotometer, to determine the vanadium content.

2.2. Synthesis of complex $\text{VO}(\text{Q}^{\text{C}6})_2$ (I)

NaOCH₃ (0.8 mmol, 43 mg) was added to a solution of $\text{HQ}^{\text{C}6}$ (0.8 mmol, 229 mg) in MeOH (10 mL) in a 50 mL flask. Then VOSO₄ (0.4 mmol, 65 mg) was solubilized in 5 mL of water and the solution was added drop by drop into the flask. The reaction was hold under magnetic stirring for 4 h in reflux conditions. After filtration, a pale yellow solid of $\text{VO}(\text{Q}^{\text{C}6})_2$ compound I, was obtained, being it partially soluble in chlorinated solvent, acetonitrile and poorly soluble in MeOH. Yield: 77 %; M.p. 255–257 °C. Elemental Analysis calcd (%) for [VO

(Q^{C6})₂: C, 64.04; H, 6.64; N, 8.79. Found: C, 64.38, H, 6.51; N, 8.84. IR (KBr, cm^{-1}): 1633 m, 1611s $\nu(\text{C}=\text{O})$, 1581vs, 1540vs $\nu(\text{C}=\text{N}+\text{C}=\text{C})$; 898vs $\nu(\text{V}=\text{O})$; 690 s, 475 m $\nu(\text{V}-\text{O})$; 659 s $\delta(\text{C}-\text{Me}) + \nu(\text{V}-\text{O})$; 627vs $\pi(\text{C}-\text{Me})$. μ_{eff} (296 K): 1.79 μ_{B} . ESI-MS ($\text{MeOH}/\text{CH}_2\text{Cl}_2$) (+): m/z (%) = 287 (15) $[\text{H}(\text{HQ}^{\text{C6}})]^+$, 309 (25) $[\text{Na}(\text{HQC}^{\text{C6}})]^+$, 360 (100) $[(\text{VO})_2\text{O}(\text{QC}^{\text{C6}})_2]^{++}$. TGA-DTA (mg% vs. °C): heating from 30 to 800 °C with a speed of 10 °C/min; at 255 °C onset fusion ($\Delta H_{\text{fusion}} = 68.29$ kJ/mol); from 290 to 490 °C progressive decomposition, with a final black residual of 10 % weight.

2.3. Synthesis of complex $\text{VO}(\text{Q}^{\text{C17}})_2$ (II)

NaOCH_3 (0.5 mmol, 27 mg) was added to a solution of HQC^{17} (0.5 mmol, 220 mg) in MeOH (8 mL) in a 50 mL flask. Then VOSO_4 (0.25 mmol, 41 mg) was solubilized in 2.5 mL of water and the solution was added drop by drop into the flask. The reaction was held under magnetic stirring for 4 h in reflux conditions. After filtration, a pale yellow solid of $\text{VO}(\text{Q}^{\text{C17}})_2$ compound II was obtained, being it soluble in chlorinated solvents and acetonitrile while only partially soluble in methanol. Yield: 84 %; M.p. 182–184 °C. Elemental Analysis calcd (%) for $[\text{VO}(\text{Q}^{\text{C17}})_2]$: C, 71.08; H, 9.16; N, 5.92. Found: C, 71.45, H, 9.07; N, 5.87. IR (KBr, cm^{-1}): 1635 m, 1614s $\nu(\text{C}=\text{O})$, 1575vs, 1537s $\nu(\text{C}=\text{N}+\text{C}=\text{C})$; 900vs $\nu(\text{V}=\text{O})$; 690 s, 482vs $\nu(\text{V}-\text{O})$; 666 m $\delta(\text{C}-\text{Me}) + \nu(\text{V}-\text{O})$; 626vs $\pi(\text{C}-\text{Me})$. μ_{eff} (296 K): 1.91 μ_{B} . ESI-MS ($\text{MeOH}/\text{CH}_2\text{Cl}_2$) (+): m/z (%) = 441 (90) $[\text{H}(\text{HQ}^{\text{C17}})]^+$, 570 (60) $[\text{VO}(\text{Q}^{\text{C17}})(\text{MeOH})_2]^+$, 946 (100) $[(\text{VO})(\text{Q}^{\text{C17}})_2\text{H}]^+$. TGA- DTA (mg% vs. °C): heating from 30 to 800 °C with a speed of 10 °C/min; at 182 °C onset fusion ($\Delta H_{\text{fusion}} = 40.41$ kJ/mol); from 300 to 520 °C progressive decomposition, with a final black residual of 18 % weight.

2.4. EPR study

Under typical conditions, the spectrometer operated at a central magnetic field of 355 mT (3550 G), scan range 110 mT (1100 G), sweep time 165 s, time constant 100 ms, modulation frequency 100 kHz, modulation amplitude 0.1 mT (1 G), at room temperature (298 K). The effective 28 mW microwave power on the samples was generated by a 280 mW microwave power source (10 dB attenuation). The analyzed samples were prepared by dissolving 1.0 mg of samples in 1.0 mL of acetonitrile, and spectra were recorded at room temperature (298 K). After addition of single drop portions of a 35 % aqueous solution of H_2O_2 to the previous solution, the successive EPR spectra were recorded, at the same temperature, after 5 min.

2.5. Catalytic oxidation in conventional solvents

1.5 mL of solvent, 0.1 mmol of sulphide (or 0.2 mmol of olefin), 1.0 mol % of catalyst and 2 equiv. of oxidant were inserted sequentially in a 5 mL flask equipped with a magnetic stirring bar, immersed in a thermostatic oil bath, at 60 °C. Further equivalents of oxidant were added stepwise at regular interval of time (1 h) during the reaction, up to 4.0 equiv. The reaction was allowed to react for different intervals of time depending on the types of used substrates. At the end of reaction, mixture was quenched with 5.0 mg of MnO_2 and, after 15 min, filtered. The progress of the reaction was monitored through GC-FID analysis, withdrawing each time an aliquot of 20 μL and adding 5 μL of *n*-hexadecane (internal standard). The oxidation products were identified by comparison of their GC retention times with those of authentic samples.

2.6. Catalytic oxidation in ionic liquids

0.1 mmol of sulphide (or 0.2 mmol of olefin) and 1.0 mol % of catalyst were added to 1.2 mL of a mixture of *n*-octane/ionic liquid 5:1 v/v for sulphides, or 1.0 mL of ionic liquid alone for olefin, respectively, in a glass vial equipped with a magnetic stirring bar, immersed in a thermostatic oil bath at 60 °C, and the biphasic mixture was stirred for

5 min. After that, 2 equiv. of oxidants are inserted into the vial. The reaction was held under heating and magnetic stirring up to 6 h, adding further equiv. of oxidant at regular interval of time (1 h) up to 4.0 equiv. and monitoring its progress through GC-FID analysis, withdrawing each time an aliquot (20 μL) of the hydrocarbon phase and adding 5 μL of *n*-hexadecane (internal standard). At the end of the reaction, the *n*-octane phase was separated, and the IL phase was washed with 3 mL of diethyl ether. The two organic phases were afterwards joined together, quenched with MnO_2 as above described, and the final solution was concentrated using a rotary evaporator, with gentle heating (40 °C), and then analysed with GC-FID.

2.7. Microwave-assisted Catalytic oxidation

The sample was prepared as above described and was inserted into the appropriate MW glass vials (0.5–2.0 mL) with the stirring bar, added with 2.0 equiv. of oxidant and then sealed. The experiment was performed under control of the temperature (70 °C), by setting the following instrumental parameters for each cycle: time = 20 min, absorption level = normal, stirring rate = 900 rpm. The progress of the reaction was monitored through GC-FID analyses. At the end of the reaction, we followed the same work-up procedure as above described.

2.8. Recycling tests of catalyst I

At the end of the first reaction cycle, using DBT as substrate and TBHP as oxidant, in a *n*-octane/BMIM- PF_6 (5:1) solvent mixture, otherwise working under the same conditions described in 2.6 section, the upper organic phase was recovered, quenched with MnO_2 as above described, and its residual sulphur content analysed by GC-FID. Next, new fresh DBT (0.1 mmol) portion in 1.0 mL of *n*-octane was added to the recycled IL phase and a new reaction cycle, started. After the fifth cycle, all the previously recovered organic phases were collected and analysed by ICP-AES, in order to evaluate the residual amount of vanadium metal, eventually due to its partial leaching.

2.9. Computational details

All the calculations were carried out adopting the following protocol. The structures were first optimized in gas-phase and characterized as minima or first order saddle points through the calculation of the mass-weighted Hessian. Since, at least in principle, different magnetic states can be involved in the present reaction, we also investigated their possible couplings.

It is important to remind that two surfaces with different spin multiplicity cross along a hyperseam whose minimum, termed as Minimum Energy Crossing Point (MECP), can be roughly considered to act as a Transition Structure (TS) for these processes termed as non-adiabatic. MECPs were obtained, in the gas-phase, using standard procedures as described elsewhere [41].

The reaction and activation free-energies at 60 °C were then calculated in the ideal gas approximation using the standard condition of 1.0 mol/liter and then corrected with the solvation free energies estimated, for CH_3CN also for CH_2Cl_2 , in the framework of Conductor-like Polarizable Continuum Model (C-PCM) [42,43].

For CH_3CN we utilized the dielectric constant of 31.0 corresponding to the value at 60 °C. All the calculations were performed using Density Functional Theory with the CAM-B3LYP functional [44] with the 6–31+G* basis set for the optimizations and the 6–311+G* for the C-PCM calculations. The vanadium has been always treated with the Hay and Wadt Effective Core Potential (ECP) [45].

Because of the semi-quantitative character of our computational investigation, due to the lack of quantitative experimental data to compare to, we did not perform any sensitivity analysis with respect to the quality of the functional and the size of the basis set.

Finally we also attempted a computational investigation of the same

reactions in ionic liquids. However our efforts were frustrated by the high complexity of the environmental effects which are very difficult to model with a mean field approximation and would require a deep investigation well beyond the scope of the present study [46].

In this respect we have only addressed some preliminary investigation on some species conceivable present in these conditions.

3. Results and discussion

3.1. Synthesis of complexes $VO(Q^{C6})_2$ and $VO(Q^{C17})_2$

Complexes $VO(Q^{C6})_2$ (**I**) and $VO(Q^{C17})_2$ (**II**) were synthesized by reacting vanadyl sulphate with the acylpyrazolones in basic methanol/water at room temperature (Scheme 1). They are pale-yellow solids stable to air with medium-to-good solubility in chlorinated solvents and acetonitrile. Complexes **I** and **II** display sharp and very different melting points to one another, in fact complex **II** melts at a temperature of 182–184 °C, much lower than that of complex **I** (255–257 °C), clearly due to the long aliphatic chain of Q^{C17} ligand in **II** that decreases the crystalline packing.

3.2. FT-IR characterization

Solid-state FT-IR spectra have been recorded for the free ligands HQ^{C6} and HQ^{C17} and their complexes $VO(Q^{C6})_2$ (**I**) and $VO(Q^{C17})_2$ (**II**). The disappearance in the spectra of **I** and **II** of the broad $\nu(O-H)$ absorption between 2800 and 2300 cm^{-1} and the shift of the $\nu(C=O)$ toward lower wavenumbers with respect to free ligands [from 1638 to 1611 cm^{-1} comparing HQ^{C6} and $VO(Q^{C6})_2$ and from 1626 to 1614 cm^{-1} comparing HQ^{C17} and $VO(Q^{C17})_2$] is in accordance with deprotonation of HQ and bidentate coordination of the O_2 -chelating face to vanadium. Moreover a structural information arises from the stretching vibration of the $\nu(V=O)$, which typically looks like a strong signal observed in the range 880–1000 cm^{-1} [47]: in fact, when a molecule of water is coordinated in *trans* position to the oxo ligand of vanadyl the $\nu(V=O)$ stretching band falls at frequencies higher than 960 cm^{-1} , whereas in the anhydrous form this band falls in the range 890–920 cm^{-1} [37,48]. Complexes **I** and **II** show the $\nu(V=O)$ at 898 and 900 cm^{-1} respectively, indicating the absence of coordinated water and in agreement with the thermogravimetric analysis where any weight loss corresponding to water molecules was detected. The lowering of the $\nu(V=O)$ value may arise from the molecular stacking in the solid state which can favour the interaction between an oxygen of the vanadyl cation with the vanadium center of another neighbour molecule, thus allowing the saturation of the sixth coordinative valence of the metal [37,49].

3.3. Magnetic measurements

The room-temperature magnetic susceptibility obtained for **I** and **II** is 1.79 BM and 1.91 BM, respectively, a typical paramagnetic behavior within the normal range for the spin only contribution of d^1 systems, where the orbital contribution is completely quenched [50].

3.4. Study of UV-vis electronic spectra

The UV-vis electronic spectra of the oxovanadium complex **I** and that of the corresponding proligand HQ^{C6} , have been performed in dichloromethane. For the ligand one main band having the maximum at a wavelength of 271 nm has been observed, within the range of $\pi-\pi^*$ transition of the phenyl group, being the peak of the $n-\pi^*$ transition of the carbonyl group in the acyl fragment (ca. 230–233 nm) not detectable inside the windows we used (Fig. 1). Upon coordination, this absorption band is red shifted to form a widened band with the maximum at 282 nm, indicating the involvement of the carbonyl group in the complex formation with the metal ion, according to the behaviour

of a series of oxovanadium(IV) 4-acyl-5-pyrazolone complexes, previously reported [37]. The analysis of UV-vis spectra of complex **I** treated with TBHP, showed a clear shift toward shorter wavelength values (from 282 to ca. 270 nm).

An attempt to rationalize the results implies that, being the most intense band ($\pi-\pi^*$ transition) moving from the complex alone to the complex activated in the presence of the oxidant (TBHP), which implies the coordination of deprotonated TBHP to the metal thus expanding the coordination sphere of vanadium(V) species (confirmed by calculations too, see Fig. 8 onward). This necessarily causes a partial weakening of the interaction between the metal and the carbonyl moiety of the ligand, thus tentatively justifying the increasing of the energy of the $\pi-\pi^*$ transition, and consequently the shift of the observed absorption. It should be noted that the UV-vis spectra of titrated solution of the oxovanadium complex **I**, remained unchanged after 24 h (Fig. 1). Interestingly, in the UV-vis solid phase spectra of both complexes **I** and **II**, all expected transitions can be assigned, namely: ca. 280 nm ($\pi \rightarrow \pi^*$), ca. 327 nm ($n \rightarrow \pi^*$), ca. 421 nm (LMCT), ca. 560 nm (*d-d*) (see Figures S.1 and S.2 in the Supplementary Material section).

3.5. Thermogravimetric analyses

Thermogravimetric analyses (TGAs), under N_2 atmosphere, were performed on **I** and **II** revealing a significative difference in their onset melting points, at 255 °C and 182 °C for **I** and **II**, respectively. This is likely due to a superior crystalline packing aptitude of complex **I** compared to **II**, in which the long aliphatic chain counteracts crystalline packing. After melting, both **I** and **II** show an initial decomposition around 280 °C and then a rapid weight loss owed to a complete thermal decomposition, leaving a small black residual (10–18 %).

3.6. EPR measurements for complexes **I** and **II**

In order to confirm, by X band EPR analyses, the rapid oxidation of vanadium from +4 to +5 oxidation state, a well-known process occurring for the oxovanadium(IV) complexes after H_2O_2 addition, we focused our attention on both complexes **I** (Fig. 2) and **II** (see Figure S.3, in the Supplementary Material section), analysed in a 1.0 M acetonitrile solution. As expected, EPR spectrum of **I** and **II**, at 298 K, exhibited an expected hyperfine structure (HFS) derived from the interaction of free electron ($3d^1$) with the magnetic nuclear moment of ^{51}V ($I = 7/2$, 99.76 % of natural abundance), thus confirming the presence of isolated V^{IV} species as applying to a mononuclear complex. In this case, the EPR signal splits into eight-fold lines of all anisotropic components (Fig. 2) with values of $g_{iso} = 1.97$ and $A_{iso} = 109.5$ G. This values could correspond to vanadyl ions (VO^{2+}) in octahedral distorted symmetry [51]. Furthermore, the *g*-value lies within the 1.9–1.99 range and agrees with the fact that when the *d*-shell is less than half filled, the spin-orbit effect reduces the *g*-value in comparison with that of a free electron (2.0023) [52]. By the same way, similar measurements were carried out on the same complex **I** after dropwise titration with a 35 % aqueous solution of H_2O_2 , in order to mimic catalytic reaction medium. The new EPR spectrum showed the disappearance of previous well defined HFS, as expected when the oxidation toward oxovanadium(V) complex derivatives, occurred (see Fig. 2, red line). Results fully comparable were obtained in the analysis of the complex.

3.7. Study of the catalytic activity

3.7.1. Selective oxidation of styrene and *cis*-cyclooctene (CO)

As model substrates for the study of the catalytic oxidation of conjugated or unconjugated olefins, we focused our attention on styrene and *cis*-cyclooctene (CO), as examples of electron poor or more electron rich olefins, respectively. With the aim of finding the best experimental parameters, provided that in accordance with our aims to work under mild conditions, we took in consideration the results previously

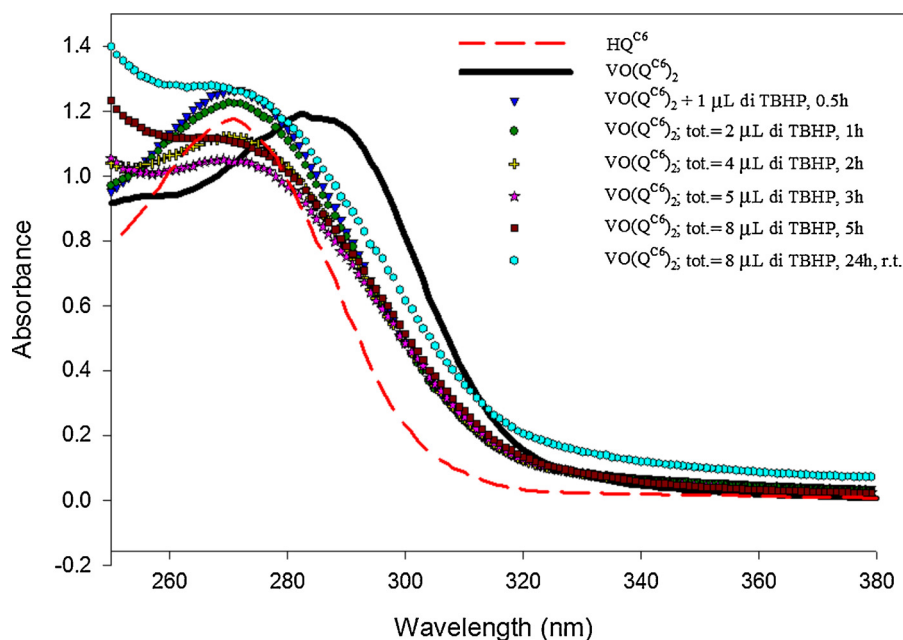


Fig. 1. Electronic spectra of HQ^{C6} and $\text{VO}(\text{Q}^{\text{C6}})_2$ (I). The reactivity of I with TBHP, is also showed. Spectra were recorded after the successive addition (1.0 μL) of 5.5 M TBHP solution in *n*-decane, to 10 mL of CH_2Cl_2 solution of I (0.4 mg).

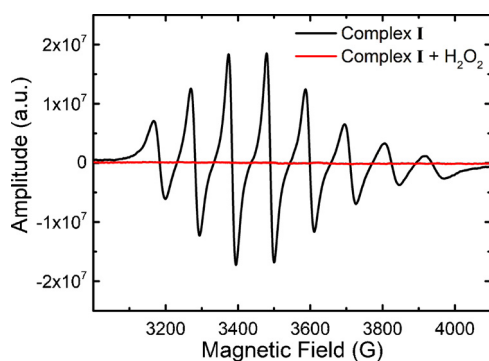


Fig. 2. EPR spectrum of oxovanadium complex I in acetonitrile, at 298 K.

obtained in the study of the catalytic oxidation of the challenging styrene, with oxovanadium(IV) complexes, promoted by hydrogen peroxide (H_2O_2) as main oxidant, working at room temperature (r.t.) [37]. Thus, after the starting optimization study, we opted for the use of aqueous H_2O_2 and either, aqueous or decane solutions of *tert*-butyl hydroperoxide (TBHP_{aq} or TBHP, respectively), as main oxidants, and acetonitrile or CH_2Cl_2 and CHCl_3 , as conventional solvents. According to our objective, we decided to work with moderate temperature (up to 60 °C) and moderate amounts of both oxidant (up to 4.0 equiv.) and catalyst (1.0 mol%), within up to 6 h of reaction time. In all experiments, the oxidant has been added *portionwise* to the reaction mixture (1.0 equiv. per hour, until the maximum amount described) to avoid its decomposition, as already reported in the case of H_2O_2 under vanadium promoted catalysis [22,53]. The experimental results obtained in the oxidation of styrene with the main observed products (Scheme 2), are summarized on Table 1.

The starting catalytic experiments, carried out with H_2O_2 in acetonitrile, gave good conversion (80–85 %) of the starting material (s.m.), irrespective to the oxovanadium complex $\text{VO}(\text{Q}^{\text{C6}})_2$ (I) or $\text{VO}(\text{Q}^{\text{C17}})_2$ (II) used, being benzaldehyde A and benzoic acid B, the main products, obtained with comparable yields (33–39 %) and selectivities (41–46 %), along with traces of acetophenone D and 1-phenylethane-1,2-diol E (Table 1, entries 1–2, and Scheme 2).

The selectivity was in accordance with results previously obtained

in the H_2O_2 promoted oxidation of styrene with high-valent oxo-metal based catalysts containing Re(VII) [54] or V(IV) [37]. Scheme 2 describes the known reaction mechanisms generally operative under the catalytic oxidation of styrene, promoted by hydroperoxides. Frequently, depending on the experimental conditions (oxidant, solvent, etc.) the styrene epoxide C is converted to the corresponding benzaldehyde A due to the H_2O_2 addition over the initially formed epoxide and successive cleavage of the hydroxyl-hydroperoxystyrene intermediate (not shown) [55]. In addition, for the two conceivable competing channels (epoxidation and oxidative cleavage, Scheme 2), previous theoretical calculations showed that, under kinetic control and with H_2O_2 excess, the epoxidation route is the less efficient process [56]. The excess of oxidant is responsible for the overoxidation of benzaldehyde A to benzoic acid B, while traces of by-products D and E come from the benzylic oxygen CH insertion/isomerization on styrene and the partial hydrolysis of the epoxide C, respectively. For what it concerns both the catalytic activity and selectivity, the two oxovanadium(IV) complexes $\text{VO}(\text{Q}^{\text{C6}})_2$ or $\text{VO}(\text{Q}^{\text{C17}})_2$ acted in a similar way, with TON ranging from 80 to 85 (Table 1, entries 1–2), being these values comparable with results previously described in literature [55]. The disappointing results observed when chlorinated solvents (dichloromethane or chloroform) are used with H_2O_2 as oxidant [25,57], have been confirmed also under our experimental conditions (Table 1, entries 3 and 5): an attempt to force the conversion of s.m. with the aid of microwave (MW) assisted heating, provided equally negative results (Table 1, entry 4). Quantum chemical calculations, carried out in the framework of Density Functional Theory (DFT), furnished a valid rationale for these experimental results (see onward). On the other hand, the use of *t*-butyl hydroperoxide (TBHP) as main oxidant, either in decane or aqueous solution (TBHP_{aq}), allowed to increase the selectivity and yield of styrene oxidation toward benzaldehyde A, both in acetonitrile and chloroform, reaching in the former solvent quantitative conversions of s.m. (Table 1, entry 6). In terms of selectivity, interesting differences between acetonitrile and chloroform have been observed. In acetonitrile, the formation of epoxide C (or the corresponding 1-phenylethane-1,2-diol E, when using TBHP_{aq} due to the epoxide hydrolysis) has been detected with comparable yield and selectivity with both catalysts I and II (Table 1, entries 7–8, vs. entry 6). Differently, in chloroform aside the main aldehyde A, a fairly good amount of acetophenone D was

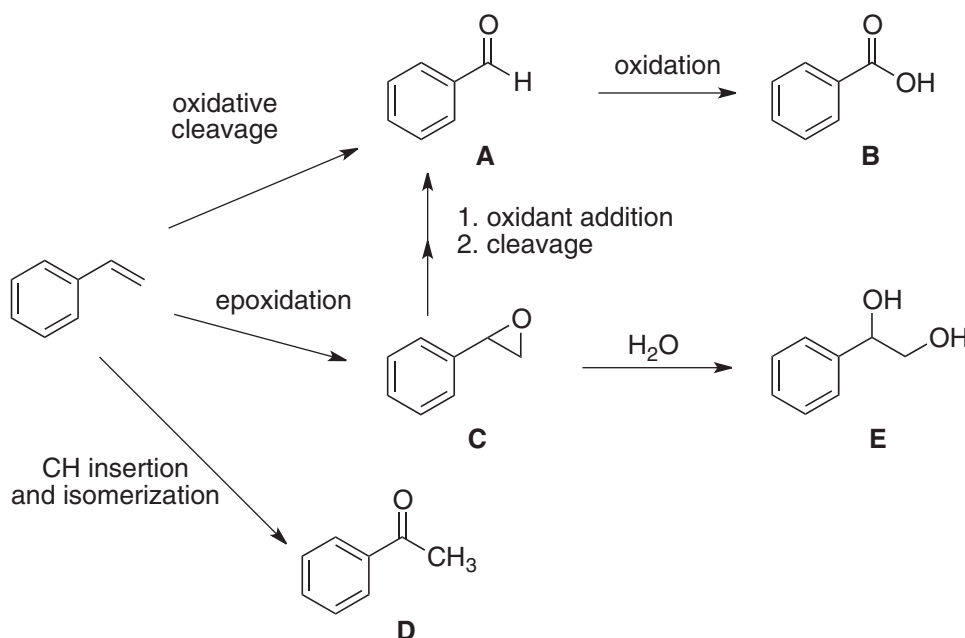


Table 1
Styrene oxidation catalysed by $\text{VO}(\text{Q}^{\text{C6}})_2$ and $\text{VO}(\text{Q}^{\text{C17}})_2$ complexes.

Entry ^a	Catalyst	Oxidant	Solvent	Conv. (%)	TON ^b	Products (% Y) ^c [% S] ^c				
						A (see Scheme 2)	B	C	D	E
1	$\text{VO}(\text{Q}^{\text{C6}})_2$	H_2O_2	MeCN	85	85	(36) [42]	(39) [46]	–	(3) [4]	(7) [8]
2	$\text{VO}(\text{Q}^{\text{C17}})_2$	H_2O_2	MeCN	80	80	(33) [41]	(34) [43]	–	(5) [6]	(8) [10]
3	$\text{VO}(\text{Q}^{\text{C6}})_2$	H_2O_2	CH_2Cl_2	3	3	(3) [100]	–	–	–	–
4 ^d	$\text{VO}(\text{Q}^{\text{C6}})_2$	H_2O_2	CH_2Cl_2	10	10	(10) [100]	–	–	–	–
5	$\text{VO}(\text{Q}^{\text{C6}})_2$	H_2O_2	CHCl_3	5	5	(5) [100]	–	–	–	–
6	$\text{VO}(\text{Q}^{\text{C6}})_2$	TBHP	MeCN	98	98	(60) [61]	(13) [13]	(25) [26]	–	–
7	$\text{VO}(\text{Q}^{\text{C6}})_2$	TBHP _{aq}	MeCN	90	90	(60) [67]	(10) [11]	–	–	(20) [22]
8	$\text{VO}(\text{Q}^{\text{C17}})_2$	TBHP _{aq}	MeCN	93	93	(61) [66]	(12) [13]	–	–	(20) [21]
9	$\text{VO}(\text{Q}^{\text{C6}})_2$	TBHP	CHCl_3	76	76	(46) [60]	(5) [7]	–	(25) [33]	–
10	$\text{VO}(\text{Q}^{\text{C17}})_2$	TBHP	CHCl_3	78	78	(43) [55]	(7) [9]	–	(28) [36]	–
11	$\text{VO}(\text{Q}^{\text{C6}})_2$	H_2O_2	BMIM-BF ₄	90	90	(29) [32]	(55) [61]	(6) [7]	–	–
12	$\text{VO}(\text{Q}^{\text{C6}})_2$	H_2O_2	BMIM-OTf	94	94	(23) [24]	(66) [70]	(5) [6]	–	–
13	$\text{VO}(\text{Q}^{\text{C6}})_2$	TBHP	BMIM-BF ₄	80	80	(15) [19]	(62) [77]	(3) [4]	–	–
14	$\text{VO}(\text{Q}^{\text{C6}})_2$	TBHP	BMIM-OTf	86	86	(20) [23]	(54) [63]	(12) [14]	–	–
15	$\text{VO}(\text{Q}^{\text{C6}})_2$	TBHP	BMIM-PF ₆	90	90	(30) [33]	(60) [67]	–	–	–
16	$\text{VO}(\text{Q}^{\text{C17}})_2$	TBHP	BMIM-PF ₆	87	87	(28) [32]	(59) [68]	–	–	–

^a Experimental conditions: styrene 0.2 mmol; catalyst = 1.0 mol%; oxidant = 4.0 equiv.; reaction time: 6 h; temperature: 60 °C; volume: 1.5 mL for conventional solvents and 1.0 mL for ILs.

^b TON (turnover number): mmols of converted substrate per mmole of catalyst.

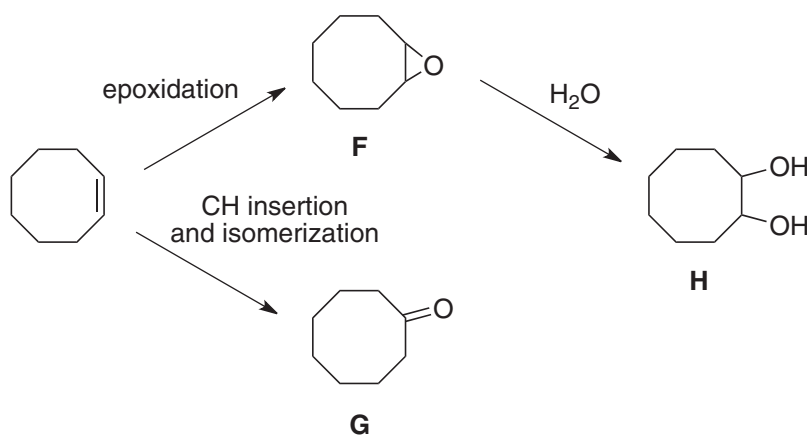
^c Y = yield; S = selectivity; yields are calculated on converted substrate.

^d MW-promoted reaction: 2 cycles of 20 min, 70 °C, absorption level = normal, stirring rate = 900 rpm.

detected, irrespective to the type of used catalyst I or II, being the conversion of s.m. lower than that in acetonitrile (Table 1, entries 9–10 vs. 6–8). In the first instance, this different outcome may be attributable to the different polarity and donor ability properties between acetonitrile (higher) and chloroform (lower), which could affect the reactivity of active species produced in consequence of the interaction among oxidant and oxovanadium complex I or II (see onward).

Having in mind to evaluate the discriminating role, if any, of common alkylimidazolium ionic liquids (ILs) like BMIM-BF₄, BMIM-PF₆ and BMIM-OTf, in terms of their hydrophilic (BMIM-OTf and BMIM-BF₄) or hydrophobic (BMIM-PF₆) properties and potential coordinating ability of their anions toward the vanadium centre (BF₄⁻ > TfO⁻ > PF₆⁻) [58], we started to study the oxidation of styrene in these solvents, with catalyst I. Then, the system formed by

H_2O_2 and complex I in hydrophilic ILs like BMIM-BF₄ and BMIM-OTf, gave the highest conversions of styrene (90–94 %), with a different selectivity between aldehyde A and benzoic acid B, the latter being obtained in major yield (55–66 %), in comparison with acetonitrile, aside traces of epoxide C (Table 1, compare entries 11–12 vs. 1–2). The study performed with TBHP showed the following order of activity BMIM-PF₆ > BMIM-OTf > BMIM-BF₄ [58], in terms of conversion of s.m., although with minor differences (ranging from 80 % to 90 %), the selectivity being the same as that in the case of H_2O_2 (Table 1, compare entries 13–15 vs. 11–12). Meaningfully, no substantial differences have been observed by using the catalyst II with hydrophobic BMIM-PF₆, concerning both the conversion of substrate and the selectivity of the oxidation (Table 1, entry 16 vs. entry 15). This could confirm that, within the oxovanadium complex, the alkyl side-chain in the acyl



Scheme 3. Main products obtained from *cis*-cyclooctene catalytic oxidation.

moiety of 4-acyl-5-pyrazolone ligands, is too far from the catalytically active metal centre to be able to somehow affect the outcome of catalytic reaction, at least in terms of different steric hindrance. Overall, it seems clear that there is no great advantage regarding the chemistry of the catalytic styrene oxidation, in the use of ILs in place of conventional solvents, being equally necessary, in both cases, an excess of oxidant (up to 4.0 equiv.) and prolonged reaction time (up to 6 h), to reach satisfying conversion values.

The oxidation of CO, catalyzed by complex **I** and **II**, was then performed with the aim of continuing the investigation of their catalytic activity, under the same experimental conditions as above described for styrene, but with a substrate characterized by the presence of a more electron-rich double bond. Also in this case, H₂O₂ showed to be less efficient, in comparison to TBHP, either with conventional solvents or ILs, irrespective to the type of catalyst **I** or **II**. Indeed, in acetonitrile, after 6 h, only moderate conversions of s.m. have been observed (65–68 %), with high selectivity for the corresponding CO epoxide **F**, being also detectable traces of 1,2-diol **H** derived from the hydrolysis of the epoxide, and cyclooctanone **G**, derived from the selective oxygen CH insertion/isomerization on the s.m. (see Scheme 3 and Table 2, entries 1–2).

Chloroform confirmed to be a poor suitable solvent with hydrogen peroxide (in spite of complete selectivity for the epoxide **F**), and no significant improvement has been achieved by using MW assisted heating (Table 2, entries 3–4). Newly, TBHP behaved as the most efficient oxidant, either in chloroform or in acetonitrile, being the former the most suitable solvent, affording quantitative epoxide formation

after only 1 h at 60 °C (Table 2, compare entry 6 vs. entry 5). The slight increased conversion observed in chloroform with respect to acetonitrile may be due, at least in part, to the donor ability of acetonitrile which could hinder the coordination of the oxidant to the vanadium center [59]. Differently, the experiments performed in ILs, namely BMIM-PF₆ and BMIM-BF₄, in general showed less reactivity in comparison to acetonitrile and chloroform, irrespective to the use of H₂O₂ or TBHP as oxidants, the conversions of s.m. ranging from 65 to 73 %, after 6 h. The main difference may be found on the complete selectivity toward epoxide **F** observed with TBHP (Table 2, entries 9–11), while with H₂O₂ the epoxide **F** was obtained with lower selectivity (64–72 %) aside lower amounts of product **G** and traces of 1,2-diol **H** (Table 2, entries 7–8). Newly, no main differences have been found in the catalytic activity between catalysts **I** and **II**, in BMIM-PF₆, confirming the trend showed in the oxidation of styrene (Table 2, entry 10 vs. 11). For the two used ILs, the following order of activity BMIM-PF₆ > BMIM-BF₄ was confirmed, even if without relevant differences [58].

3.7.2. Selective oxidation of DBT and DMDBT

The growing interest towards the chemistry of oxovanadium(IV) complexes and their use in environmentally relevant catalytic industrial processes, such as Oxidative Desulfurization (ODS) [60], for the achievement of Ultra-Low-Sulphur-Diesels (ULSDs), has led us to test the catalytic activity of our catalysts VO(Q^{C6})₂ (**I**) and VO(Q^{C17})₂ (**II**), for the oxidations of aromatic sulphides. Dibenzothiophene (DBT) and 4,6-dimethyldibenzothiophene (DMDBT) substrates have been chosen as models of aromatic sulphur compounds contained in crude oil.

Table 2
Cis-cyclooctene oxidation catalysed by VO(Q^{C6})₂ (**I**) and VO(Q^{C17})₂ (**II**).

Entry ^a	Catalyst	Oxidant	Solvent	Time (hours)	Conv. (%)	TON ^b	Products (% Y) [% S] ^c (see Scheme 3)
1	VO(Q ^{C6}) ₂	H ₂ O ₂	MeCN	6	68	68	F: (63), [93]; G: (3), [4]; H: (2), [3]
2	VO(Q ^{C17}) ₂	H ₂ O ₂	MeCN	6	65	65	F: (59), [91]; G: (3), [5]; H: (3), [4]
3	VO(Q ^{C6}) ₂	H ₂ O ₂	CHCl ₃	6	3	3	F: (3), [100]
4 ^d	VO(Q ^{C6}) ₂	H ₂ O ₂	CHCl ₃	< 1 ^e	19	19	F: (19), [100]
5	VO(Q ^{C6}) ₂	TBHP	MeCN	1.5	98	98	F: (98), [100]
6	VO(Q ^{C6}) ₂	TBHP	CHCl ₃	1	> 99	100	F: (> 99), [100]
7	VO(Q ^{C6}) ₂	H ₂ O ₂	BMIM-PF ₆	6	70	70	F: (45), [64]; G: (20), [29]; H: (5) [7]
8	VO(Q ^{C6}) ₂	H ₂ O ₂	BMIM-BF ₄	6	65	65	F: (47), [72]; G: (14), [22]; H: (4) [6]
9	VO(Q ^{C6}) ₂	TBHP	BMIM-BF ₄	6	69	69	F: (69), [100]
10	VO(Q ^{C6}) ₂	TBHP	BMIM-PF ₆	6	73	73	F: (73), [100]
11	VO(Q ^{C17}) ₂	TBHP	BMIM-PF ₆	6	71	71	F: (71), [100]

^a Experimental conditions: *cis*-cyclooctene 0.2 mmol; catalyst = 1.0 mol%; oxidant = 2.0 equiv.; temperature: 60 °C; solvent: 1.5 mL for conventional solvents and 1.0 mL for ILs.

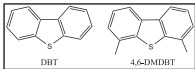
^b TON (turnover number): mmoles of converted substrate per mmole of catalyst.

^c Y = yield; S = selectivity; yields are calculated on converted substrate.

^d MW-promoted reaction: 2 cycles of 20 min, 70 °C, absorption level = normal, stirring rate = 900 rpm.

^e Time of reaction = 40 min.

Table 3
DBT and DMDBT oxidation catalysed by VO(Q^{C6})₂ and VO(Q^{C17})₂ complexes.

Entry ^a	Substrate	Catalyst	Oxidant	Solvent	Conv. (%)	TON ^b	(Products) ^c (% Y), [% S]
							
1	DBT	VO(Q ^{C6}) ₂	H ₂ O ₂	MeCN	92	92	(SO ₂) (92), [100]
2	DBT	VO(Q ^{C6}) ₂	H ₂ O ₂	CH ₂ Cl ₂	70	70	(SO) (30), [43] (SO ₂) (40), [57]
3	DBT	VO(Q ^{C6}) ₂	TBHP	MeCN	> 99	100	(SO ₂) (> 99), [100]
4	DBT	VO(Q ^{C6}) ₂	H ₂ O ₂	BMIM-OTf ^d	65	65	(SO ₂) (65), [100]
5	DBT	VO(Q ^{C6}) ₂	TBHP	BMIM-OTf ^d	96	96	(SO ₂) (96), [100]
6	DBT	VO(Q ^{C6}) ₂	TBHP	BMIM-BF ₄ ^d	90	90	(SO ₂) (90), [100]
7	DBT	VO(Q ^{C6}) ₂	TBHP	BMIM-PF ₆ ^d	> 99	100	(SO ₂) (> 99), [100]
8	DBT	VO(Q ^{C17}) ₂	TBHP	BMIM-BF ₄ ^d	80	80	(SO ₂) (80), [100]
9	DBT	VO(Q ^{C17}) ₂	TBHP	BMIM-PF ₆ ^d	96	96	(SO ₂) (96), [100]
10	DMDBT	VO(Q ^{C6}) ₂	H ₂ O ₂	MeCN	80	80	(SO) (30), [37] (SO ₂) (50), [63]
11	DMDBT	VO(Q ^{C6}) ₂	H ₂ O ₂	CH ₂ Cl ₂	75	75	(SO) (55), [73] (SO ₂) (20), [27]
12	DMDBT	VO(Q ^{C6}) ₂	TBHP	MeCN	95	95	(SO ₂) (95), [100]
13	DMDBT	VO(Q ^{C6}) ₂	TBHP	BMIM-OTf ^d	94	94	(SO) (8), [9] (SO ₂) (86), [91]
14	DMDBT	VO(Q ^{C6}) ₂	TBHP	BMIM-BF ₄ ^d	83	83	(SO) (12), [14] (SO ₂) (71), [86]
15	DMDBT	VO(Q ^{C6}) ₂	TBHP	BMIM-PF ₆ ^d	> 99	100	(SO) (10), [10] (SO ₂) (89), [90]
16	DMDBT	VO(Q ^{C6}) ₂	TBHP	BMIM-PF ₆	96	96	(SO) (18), [19] (SO ₂) (78), [81]

^a Experimental conditions: substrate 0.1 mmol; catalyst = 1.0 mol%; oxidant = 4.0 equiv.; temperature: 60 °C; reaction time: 4 h.

^b TON (turnover number): mmoles of converted substrate per mmole of catalyst.

^c SO = sulfoxide; SO₂ = sulfone. Y = yield; S = selectivity; yields are calculated on converted substrate.

^d 1.2 mL of *n*-octane/IL = 5:1 mixture.

During combustion they produce SO_x derivatives that are able to affect the atmospheric ozone layer, increasing the formation of acid rains, and reducing the life of the engine due to corrosion. Thus, their complete removal due to their complete oxidation to sulfones and successive extraction with a selected solvent (extractive catalytic oxidative desulfurization, ECODS), represents one of the most demanding challenges from an environmental point of view [61,62]. Among others, one of the most studied class of solvents, within the ECODS technique, is represented by ILs [58,63,64].

In order to mimic the hydrophobicity of a real crude oil, the catalytic activity of complexes I and II, were studied in a 5:1 mixture of *n*-octane/IL, instead of pure IL phase. Moreover, for sake of comparison with the above reported study on olefin oxidation, we tested the model ODS reactions also in acetonitrile and dichloromethane. In the Table 3 are reported the main results we have obtained in this study. Acetonitrile gave the best results, affording quantitative conversion of dibenzothiophene (DBT) and complete selectivity toward the corresponding sulfone, with catalyst I (Table 3, entry 3). With the same catalyst I, hydrogen peroxide showed a slight reduction of activity, in acetonitrile (vs. TBHP), while in dichloromethane this oxidant gave both lower activity and selectivity still being present, after 4 h, about 30 % of unreacted s.m. and 30 % of sulfoxide, in the crude (Table 3, entries 1–2). Anyway, also with a hydrophilic IL like BMIM-OTf, H₂O₂ confirmed to be less efficient in comparison to TBHP, only affording a moderate 65 % of s.m. conversion, but with complete selectivity for the sulfone (Table 3, entry 4). A detailed investigation of the activity of complex I, in the selective DBT oxidation with TBHP by using all the selected ILs, namely BMIM-BF₄, BMIM-OTf and BMIM-PF₆, confirmed almost quantitative conversion of s.m. and most notably, complete selectivity for the sulfone formation (Table 3, entries 5–7).

The complex II confirmed a high catalytic activity for the oxidation of DBT, even if with a slight reduction in the efficiency in comparison with the complex I (Table 3, compare entries 8–9 vs. entries 6–7). The following order of activity, for ILs, BMIM-PF₆ > BMIM-OTf > BMIM-BF₄, observed in DBT oxidation, is the same as that observed during

olefins oxidation, thus probably confirming the role exerted by the coordinating ability (toward the metal centre) of the different ionic liquid anions in the modulation of the catalytic activity of the core vanadyl cation (VO)²⁺, within the complexes I and II, thus influencing its ability over the coordination with the main oxidants (H₂O₂ or TBHP) in the beginning of the activation step (see onward the next theoretical calculations paragraph).

On the whole, in the case of 4,6-dimethyl-dibenzothiophene (DMDBT), the presence of alkyl substituents on the 4- and 6-positions of the aromatic ring could have a double antagonistic effect, thus influencing its reactivity in consequence of either, their inductive releasing effects or their steric concerns. Indeed, with the increase of electron density on sulphur atom, an increase of the reactivity toward sulphur oxidation is generally observed [65]. On the other hand, the substituents steric effects could greatly reduce the tendency of sulphur to be oxidized, especially with systems containing sterically demanding groups. These issues are of particular interest, since the previously reported catalytic systems for ODS process, containing vanadium or tungsten metals, showed to be sensible to steric effects [66,67]. In effect also in our study, working with the selected complex I, the oxidation of DMDBT showed to be, in general, less selective in comparison to DBT, that is a mixture of sulfoxide and sulfone derivatives has been always detected, with the only exception of the TBHP/MeCN system, where the complete selectivity toward the corresponding sulfone, was observed (Table 3, entry 12). With H₂O₂, the DMDBT oxidation in acetonitrile or dichloromethane, respectively, showed comparable conversions of s.m. (from 75 % to 80 %), being the selectivity for the sulfone higher in the former solvent (Table 3, compare entry 10 vs. entry 11). Newly, when TBHP and an imidazolium ILs medium are present (as *n*-octane/IL = 5:1 mixture) the same order of activity, i.e. BMIM-PF₆ > BMIM-OTf > BMIM-BF₄, previously observed for the DBT oxidation, was confirmed also with DMDBT, with selectivity values for the sulfone ranging from 86 % to 91 % (Table 3, entries 13–15). Finally, a catalytic test performed by using the most active IL, that is BMIM-PF₆ as the unique solvent phase, to evaluate the role of *n*-octane, if any, on either

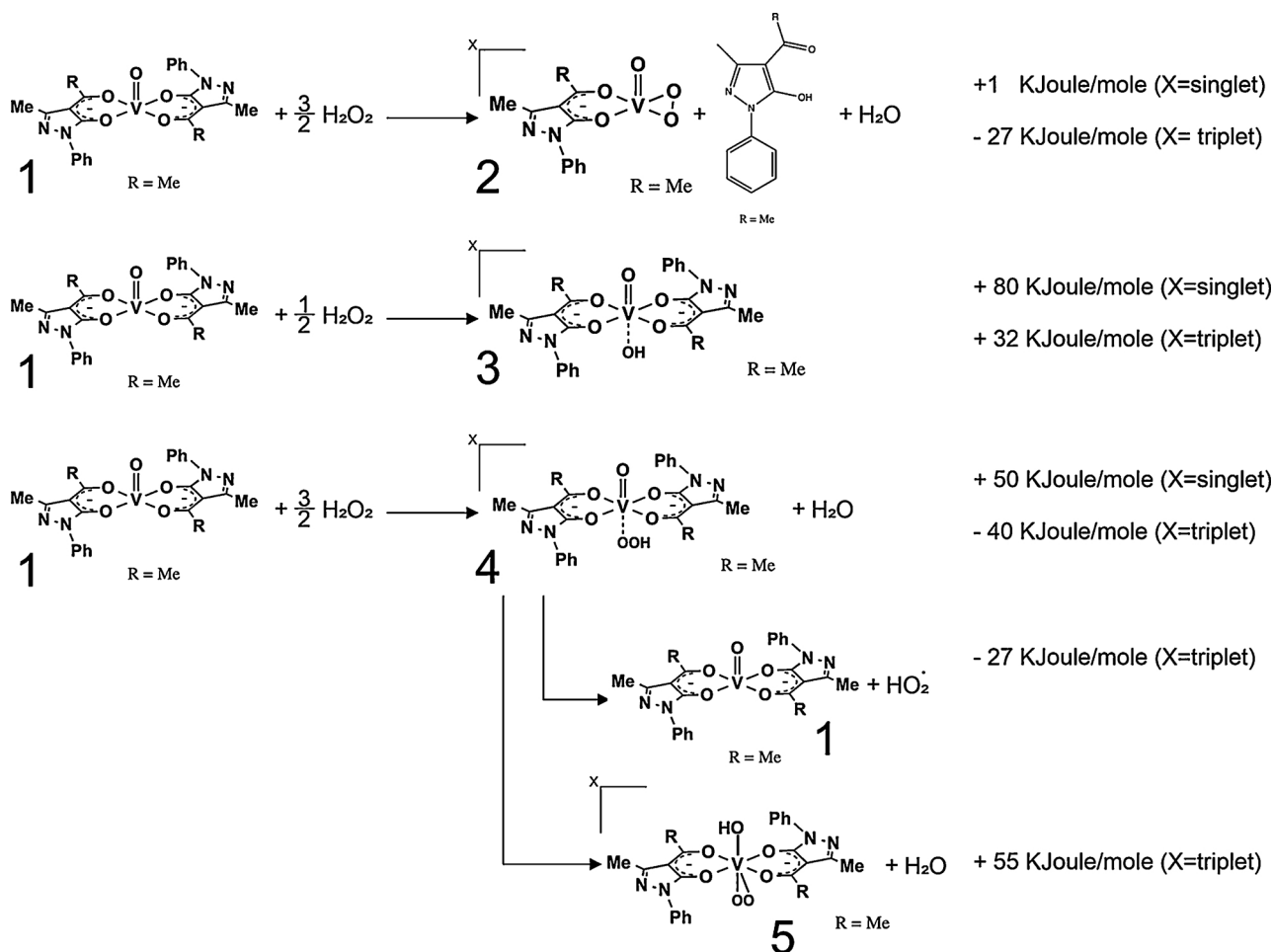


Fig. 3. Reaction free energies at 60 °C in CH₃CN solution.

the activity or selectivity of the DMDBT oxidation, furnished very similar results with other cases (Table 3, compare entry 16 vs. entries 13–15). The last result confirmed that the positive role of ILs as an extracting medium of the more polar sulfoxide and sulfones, at comparable conditions of catalytic activity, is well operative also in the *n*-octane/IL = 5:1 mixture we used, thus taking an advantage in economic terms for the lower consumption of IL, and being the system more representative of the real medium encountered with an authentic oil sample in the ODS process.

3.7.3. Recyclability experiments

The recyclability of the catalytic system was studied for the DBT oxidation with the catalyst I in a *n*-octane/BMIM-PF₆ (5:1) mixture, promoted by TBHP (see above the 2.8 section). It should be underlined that the vanadium complex retained its activity thus allowing its recyclability. After the first cycle, the organic phase was recovered and analysed by GC-FID to evaluate its residual sulphur content. Then, new fresh portions of reagent were added to the recycled IL phase containing the entrapped catalyst, and a new cycle started. Since the first cycle, trace of a white precipitate was detected in the mixture, which increased in the course of the next recycling steps. It was removed and analysed, by FTIR, after the fourth recycling cycle, showing the characteristic absorption bands of sulfone group [65]. Interestingly, the catalytic system retained the original activity, without a detectable catalyst leaching, at least for the first five cycles, showing only a very slight decreasing of activity after the third and fourth recycle (less than 10 % overall). This result may be rationalized, at least in part, as a consequence of the immobilizing aptitude of the ionic liquid medium toward either the catalytic species or the corresponding active

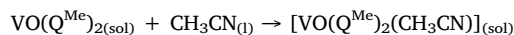
derivatives, thus allowing its stabilization and therefore its recyclability [68]. As further confirmation of this, all the collected *n*-octane phases, recovered after each recycling step, were evaporated and analysed by ICP-AES, in order to evaluate the residual amount of vanadium. The detected amount of metal confirmed that, after five running steps, only a slight leaching (8.5 %) of vanadium occurred, in comparison to the starting value.

3.8. DFT computational studies

All the results reported in this section refer to the catalyst VO(Q^{Me})₂ in which the alkyl chains C₆H₁₃ and C₁₇H₃₅ (see I and II, Scheme 1) were substituted with the methyl group in order to reduce the already high complexity of the problem. The Cartesian coordinates of all the optimized species are reported in the Supplementary Material section (Table S-1).

3.8.1. Catalyst characterization

In order to assess the most stable form of the catalyst present at 60 °C in acetonitrile, at least according to our model, we have preliminarily evaluated the possibility of finding a solvent molecule in the sixth coordination position of vanadium. At this purpose we have calculated the free energy associated to the reaction:



Which turned out to be equal to 13 kJ/mol.

For this calculation we have utilized the density of CH₃CN of 17.9 mol/liter at 60 °C.

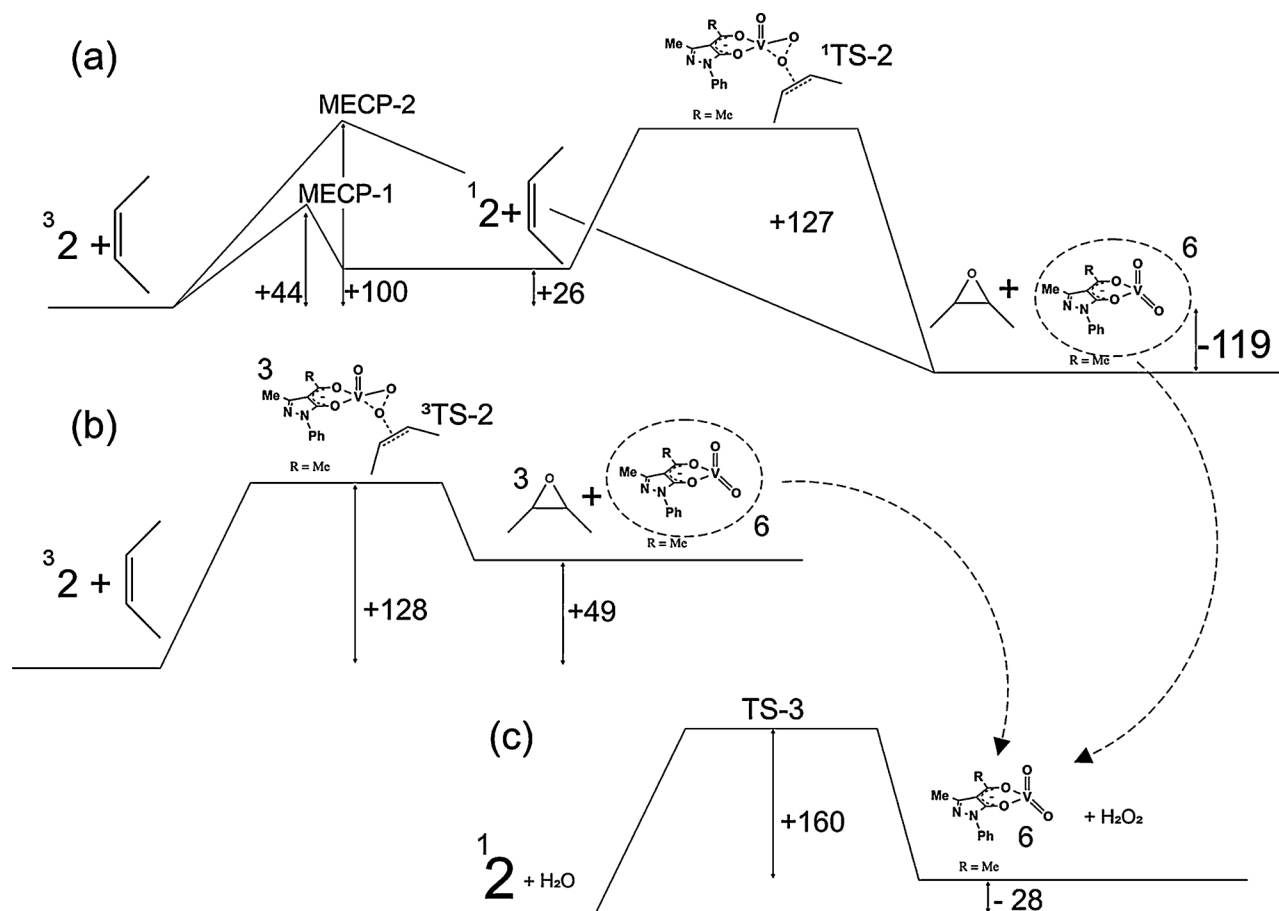


Fig. 4. Free energy diagram (in kJoule/mole) at 60 °C in CH_3CN solution of the reactions of $^3\mathbf{2}$ with olefin along the singlet (inset a) and the triplet (inset b) magnetic state. In the inset (c) we also report the free energy profile for the reformation of $^1\mathbf{2}$. Note that the channel in the inset (c) should be read from right to left.

This value allowed us to approximately consider, at least within our model, $\text{VO}(\text{Q}^{\text{Me}})_{2(\text{sol})}$ as the species mainly present in solution and hence it has been used as starting point in all the subsequent calculations.

3.8.2. Reaction with H_2O_2

First of all we have addressed the question concerning the species actually present in CH_3CN solution at the equilibrium when $\text{VO}(\text{Q}^{\text{Me}})_2$ is mixed with H_2O_2 at the temperature of the experiment.

According to the schemes reported in Fig. 3, the only species expected to be formed with a relevant yield, and containing the metal in the highest oxidation state (+5), are the peroxy $\text{VO}(\text{Q}^{\text{Me}})(\text{O}_2)$ ($\mathbf{2}$), mainly but not uniquely in the triplet state, and the hydroperoxy $^3\text{VO}(\text{Q}^{\text{Me}})_2(\text{OOH})$ ($\mathbf{3}$). This latter species also reveals thermodynamically unstable toward the formation of the HO_2^\cdot radical (see below). Our mechanistic hypothesis, in the case of H_2O_2 , is then based on these two species and the results (*i.e.* the free energy diagrams) are described in Fig. 4 with the olefin (modelled using *cis*-2-butene), and in Fig. 5 with DBT, as substrates.

For the reaction of $\mathbf{2}$ with the olefin, we localized a Sharpless-like mechanism both involving the triplet and the singlet magnetic state (Fig. 4, inset (a) and (b), and Fig. 6). $^3\mathbf{2}$ can form the dioxo $\text{VO}(\text{Q}^{\text{Me}})(\text{O})$ species ($\mathbf{6}$) and the epoxide either in the triplet state, through an adiabatic route involving $^3\text{TS-2}$, or in the singlet state through a non-adiabatic route involving **MECP-2**. The species $\mathbf{6}$ $\text{VO}(\text{Q}^{\text{Me}})(\text{O})$, further reacting with H_2O_2 , can finally restore $\mathbf{2}$ in the singlet magnetic state (Fig. 4, inset (c) and Fig. 6, Scheme Ia) which eventually either continues the reaction more efficiently (Fig. 4, inset (a), Fig. 6, Scheme Ia) or non-adiabatically regenerate $^3\mathbf{2}$ through **MECP-1**. A very similar

mechanism, with a slightly lower activation free-energy for $^1\text{TS-2} - \mathbf{4}$ species, is also found for the reaction of $\mathbf{2}$ with DBT, as reported in Fig. 5, inset (a), (b) and (c) and Fig. 6, Scheme Ib.

In this case the only difference emerged, with respect to the previous case, is the absence of **MECP-2** hence preventing the route – in principle possible but practically not very efficient also in the reaction with the olefin – directly forming the oxidation products starting from $^3\mathbf{2}$ and the olefin.

It is very important to remark that all the above processes involve the dioxocomplex $\mathbf{6}$ as a key-intermediate for the conclusion of the catalytic cycle. However this latter step requires a relatively high barrier of 160 kJoule/mole. For this reason the kinetic-mechanistic role of the processes initiated by $^1\mathbf{2}$ and/or $^3\mathbf{2}$ according to our model, might be not very efficient.

Consequently, although aware of the previously remarked intrinsic thermodynamic instability to form HO_2^\cdot radical, we have searched for an alternative route initiated by the species $\mathbf{3}$.

Also for this species we localized a Sharpless-like mechanism taking place only along the triplet magnetic state, as depicted in Fig. 7, both using olefin (inset a) and DBT (inset c) as the substrate. Moreover, if we compare the free energy barriers reported in Figures 4, 5 and 7, we can conclude that the species $\mathbf{3}$, although kinetically unstable toward the unimolecular formation of HO_2^\cdot radical, appears as much more efficient than $\mathbf{2}$.

3.8.3. Reaction with TBHP

When H_2O_2 is substituted by TBHP, the whole reaction picture undergoes a significant change. As a matter of the fact, as reported in Fig. 8, we observe that the only species present in acetonitrile solution,

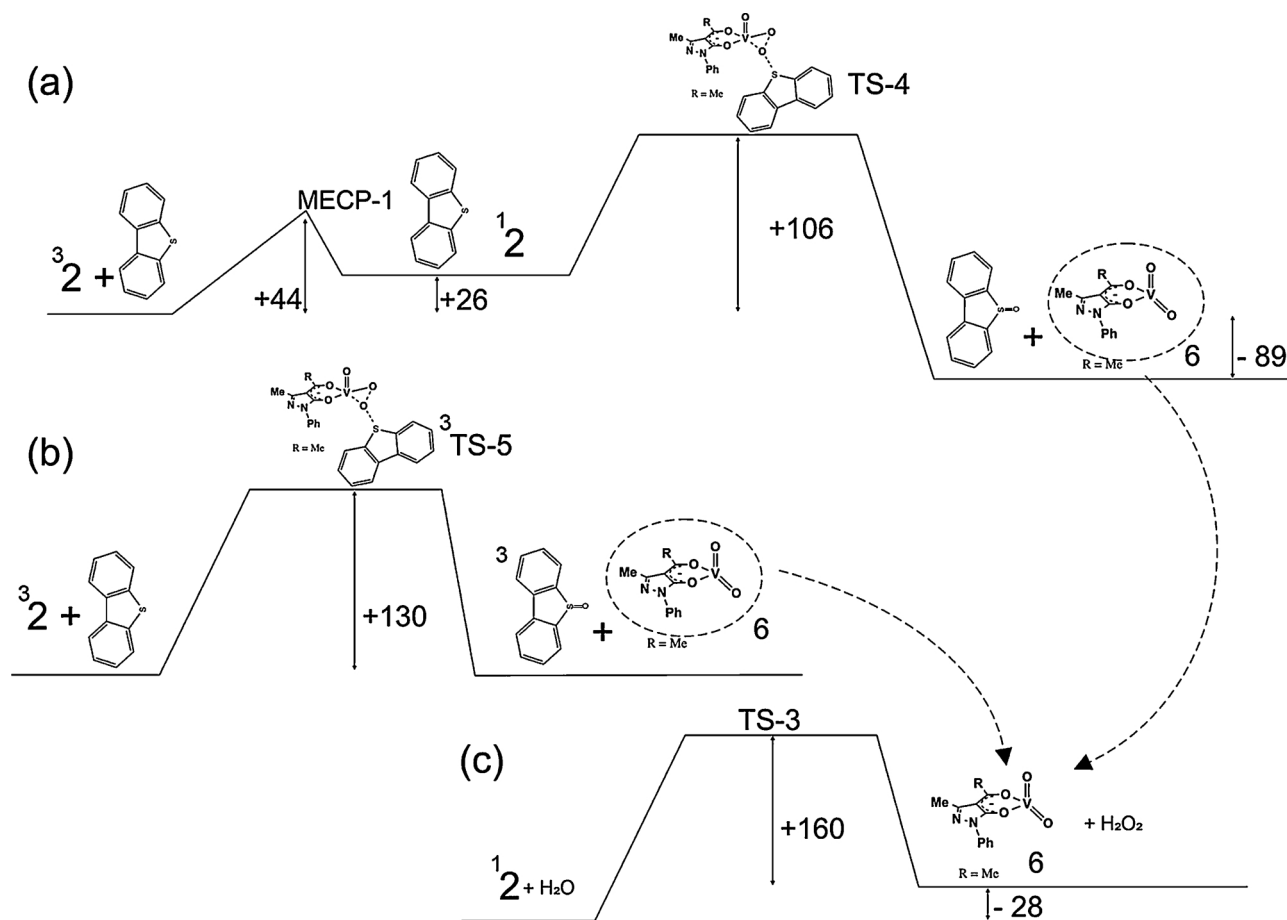


Fig. 5. Free energy diagram (in kJoule/mole) at 60 °C in CH₃CN solution of the reactions of ³2 and ¹2 with DBT along the singlet (inset a) and the triplet (inset b) magnetic state. In the inset (c) we again report the free energy profile for the reformation of ¹2. Note that the channel in the inset (c) should be read from right to left.

at the equilibrium, before the addition of the substrate, is the adduct ³4_{TBHP}.

Differently from the analogue species formed when H₂O₂ is used (i.e. the species ³4) the species

³4_{TBHP} doesn't show any propensity to dissociate hence resulting rather stable both thermodynamically and kinetically. Moreover, this species represent the only plausible intermediate able to react as reported in Fig. 9. Interestingly, the same *tert*-butylperoxovanadium(V) complex ⁴4_{TBHP} active in the catalytic oxidation of unsaturated fatty acid

methyl esters promoted by TBHP, has been previously observed by ESI-MS study [39].

Both in the case of the olefin (Fig. 9, inset a) and DBT (Fig. 9, inset b) the reaction turns out to take place onto the triplet magnetic surface through a rather Sharpless-like epoxidation mechanism followed by the regeneration of ³4_{TBHP} through the reoxidation of ³3_{TBHP}. Comparing the related free-energy barriers with the ones observed in the case of the homologous reaction of Fig. 7, we interestingly infer that the reaction with TBHP is expected to be more efficient than that with H₂O₂

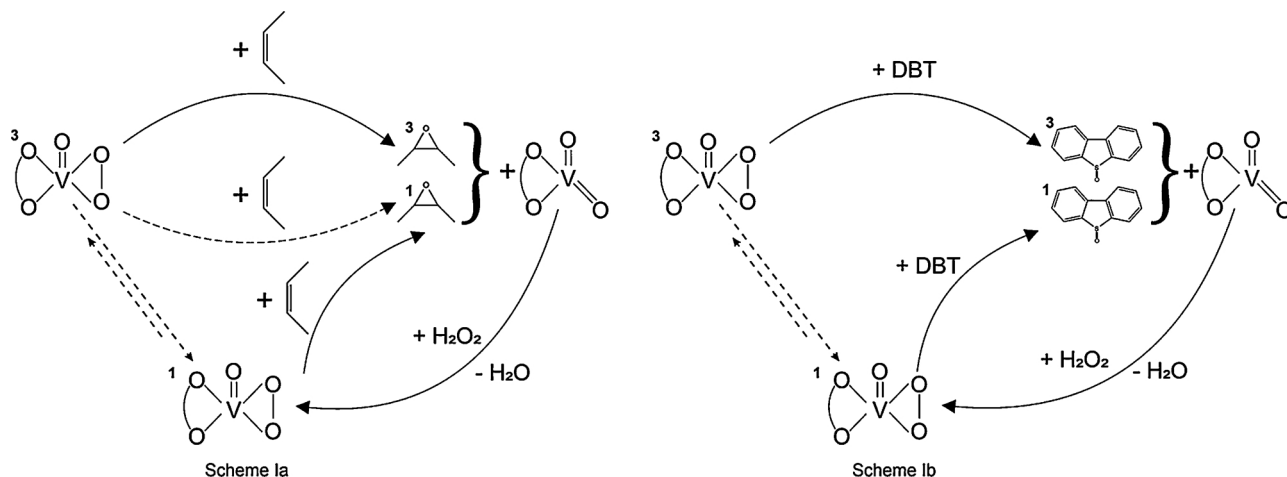


Fig. 6. Schematic and concise representation of the catalytic cycles as obtained from our calculations (see Figs. 3 and 4, respectively). The dotted arrows refer to non-adiabatic channels.

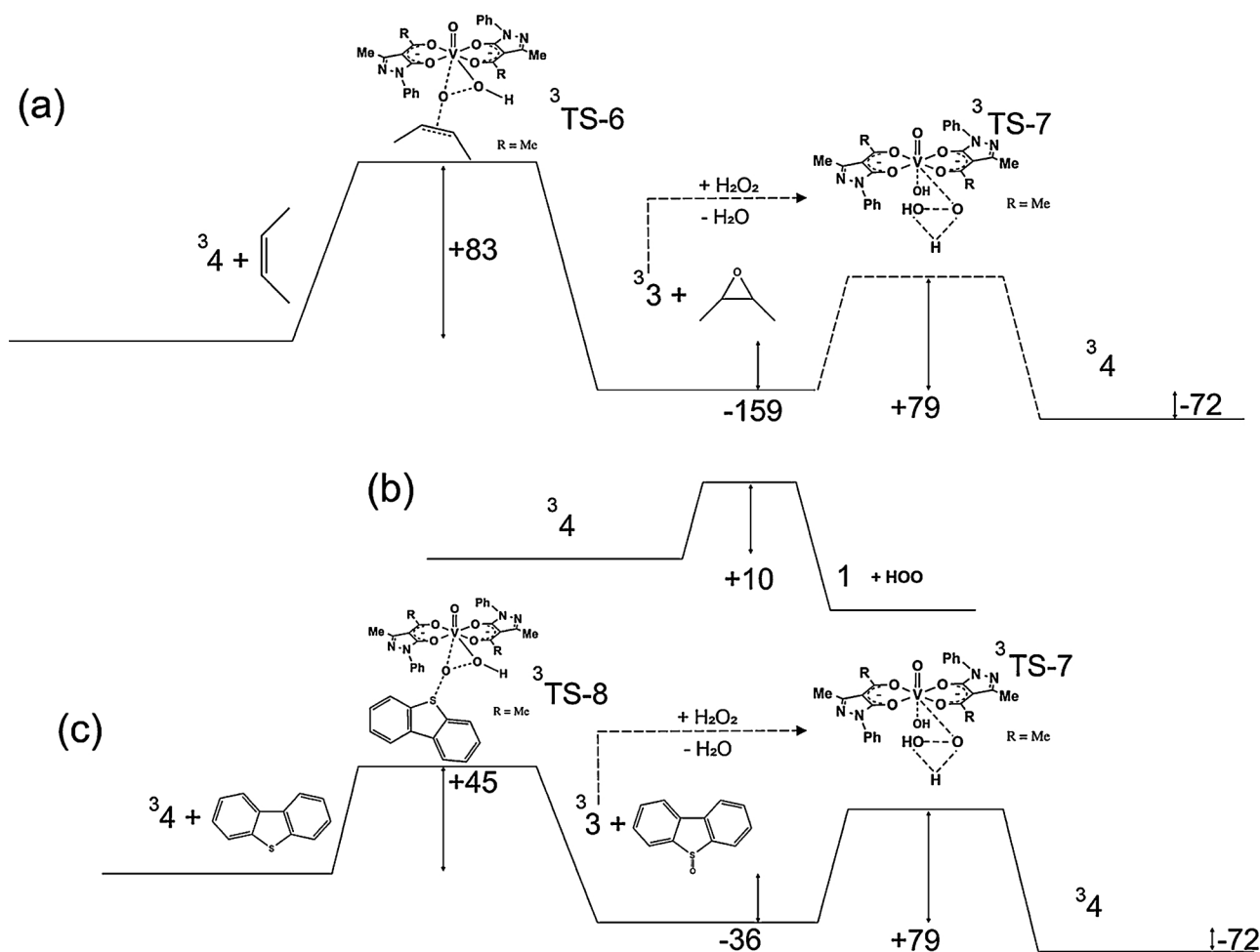


Fig. 7. Free energy diagram (in kJoule/mole) at 60 °C in CH₃CN solution of the reactions of ³4 with the olefin (inset a) and DBT (inset c). In the inset (b) we also report the free energy profile for the ³4 dissociation reaction. Note that the free energy diagram depicted with the dotted line refers to the reaction between ³3 and H₂O₂.

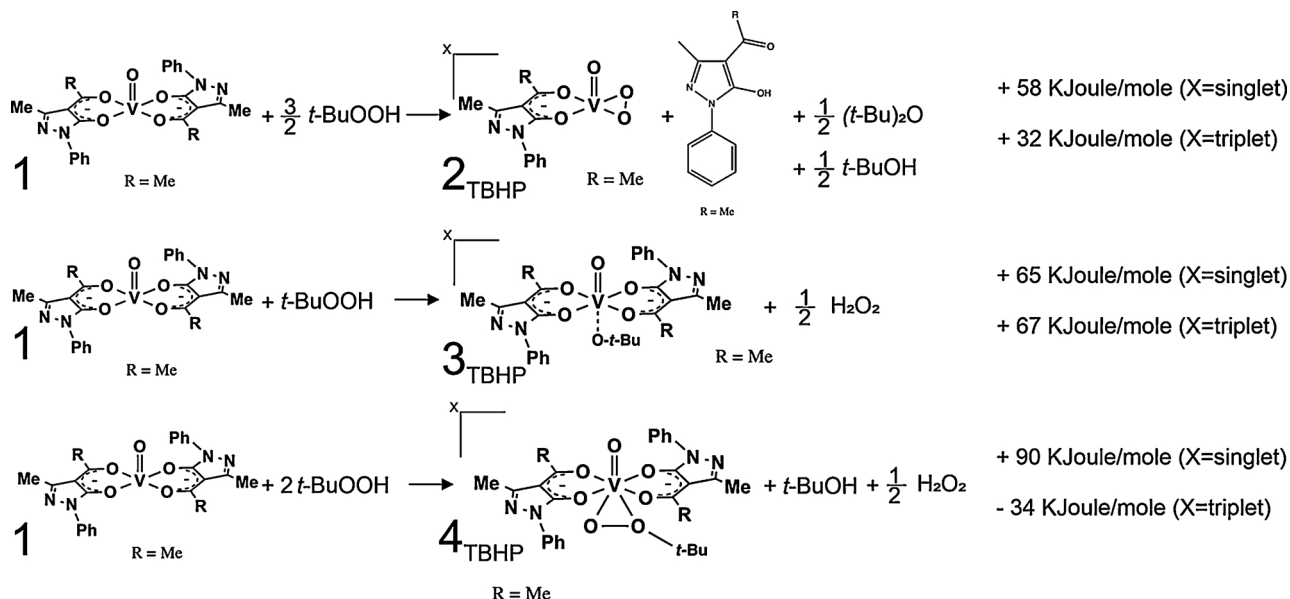


Fig. 8. Reaction free energies at 60 °C in CH₃CN solution.

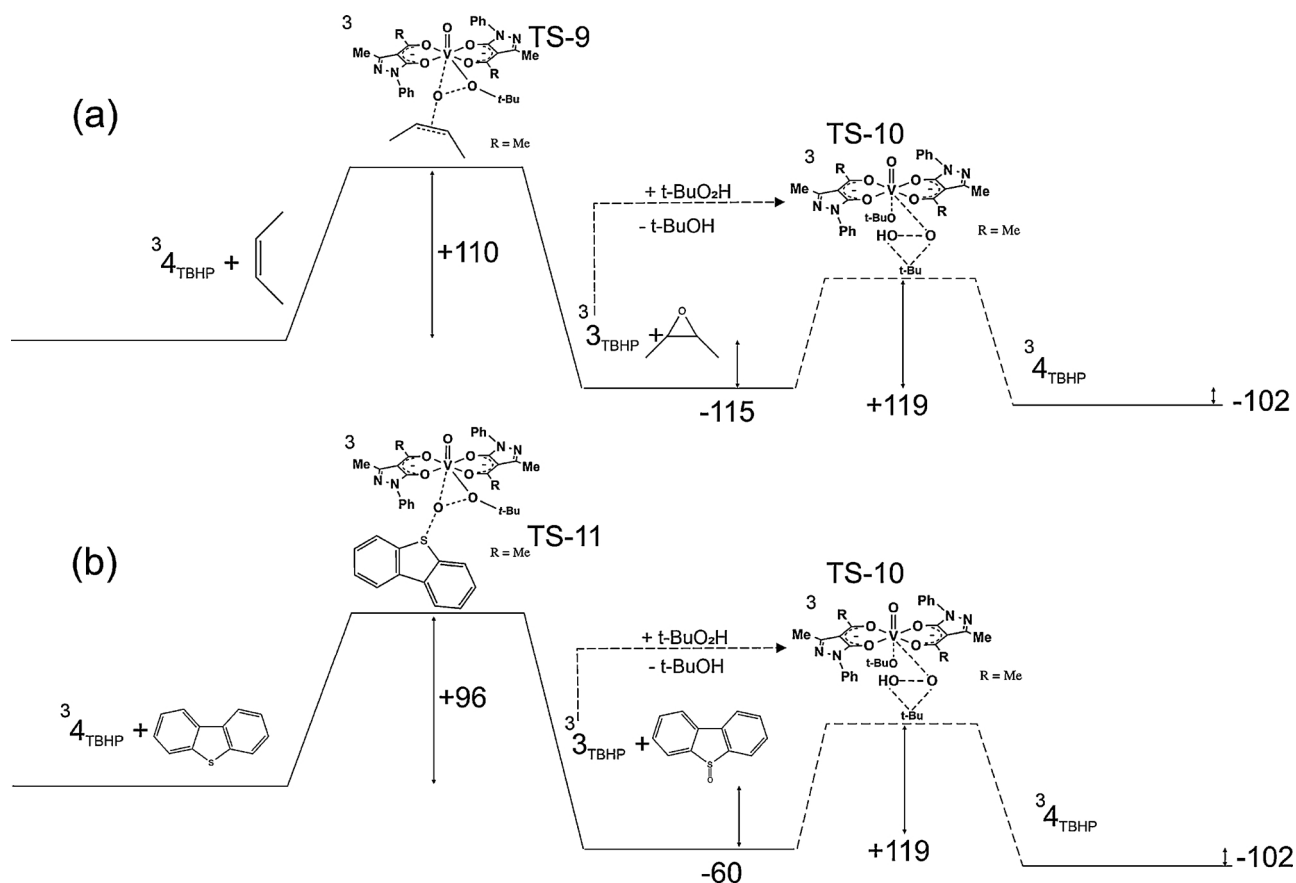


Fig. 9. Free energy diagram (in kJoule/mole) at 60 °C in CH₃CN solution of the reactions of ³4_{TBHP} with the olefin (inset a) and DBT (inset b). Note that the free energy diagram depicted with the dotted line refers to the reaction between ³3_{TBHP} and t-BuOOH.

because of the much higher kinetic stability of ³4_{TBHP} which, hence, represents the key intermediate of the whole process.

The same calculations were also carried out using CH₂Cl₂ as solvent. The results, not reported for the sake of brevity, did not show any appreciable difference with acetonitrile. As a matter of the fact, the barrier heights as well as the relative thermodynamic stability of the involved species only undergo variations within a few kJoule/mole.

As a consequence, we used a different viewpoint to interpret the reduced efficiency of H₂O₂ in CH₂Cl₂ experimentally observed. At this purpose we calculated the partition coefficient, log(P_{CH₂Cl₂/water}) and log(P_{CH₃CN/water}) of H₂O₂ and TBHP at 60 °C using the excess free energies already adopted for the calculations of the reaction energies above shown. The obtained values of log(P_{CH₂Cl₂/water}) for H₂O₂ and TBHP equal to -0.64 and -0.45, respectively, clearly indicate that the concentration of H₂O₂ is approximately half of the concentration of TBHP in this solvent. On the other hand, in the case of log(P_{CH₃CN/water}) we obtained almost identical values of -0.060, for both the oxidants. In the light of these data, we can tentatively state that the reduced catalytic activity of H₂O₂ observed in CH₂Cl₂ might be predominantly ascribed both to its reduced concentration and to its intrinsic reactivity.

3.8.4. Preliminary investigations concerning ionic liquids

As already remarked in the section dedicated to the computational details, the use of a mean field approximation in ionic liquids is much more problematic than conventional liquids. In fact in this latter environment, the neglect of the particle (explicit) description of the closest solvation shells, although physically questionable, in some cases can provide good results. This is basically impossible for ionic liquids in which the cybotactic effects can be more important. For this reason we limited our attention on the possible formation of species, emerging from a coordination bond between vanadyl [(VO)²⁺] cation and the

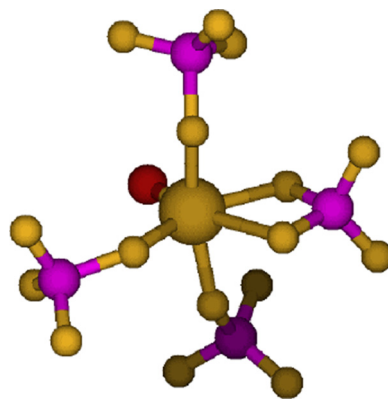


Fig. 10. Schematic picture of the [VO(BF₄)₄]²⁻ species.

BF₄⁻ anion used in some of the experimental data reported in this study. In Fig. 10 we report the picture of optimized structure of [VO(BF₄)₄]²⁻ which revealed rather stable (in gas-phase) showing an average V–F bond energy of 580 kJoule/mole lower than the V–O bond energy of 650 kJoule/mole.

However, such a difference in the binding energy might be not sufficient to resist the mass effect, due to the very high concentration of the BF₄⁻ species in the ionic liquid, leading to a partial (or even quantitative) breakdown of the catalyst hence explaining the experimentally observed moderate activity. This part of our study certainly deserves further investigation.

4. Conclusions

Two new oxovanadium(IV) complexes with 4-acyl-5-pyrazolonate- κ^2 -O,O' bidentate ligands bearing aliphatic substituents have been prepared and fully characterized both in the solid and solution state. Their catalytic potentials have been thoroughly investigated aiming to evaluate the role, if any, of the reaction medium (imidazolium based ILs vs acetonitrile or chlorinated solvents) on steering the activity and selectivity of the oxidation reactions of olefins like styrene and *cis*-cyclooctene, or organosulphur substrates as DBT and DMDBT, promoted in the presence of H₂O₂ or TBHP as main oxidants. As a whole, TBHP worked better than H₂O₂ in the activation of catalysts **I** and **II**, affording almost in all cases quantitative conversions, regardless of the type of substrates (olefins or organosulphur derivatives) or reaction medium, acetonitrile being the best one. No significant differences in terms of catalytic activity or selectivity have been detected between the two oxovanadium complexes **I** and **II**, neither in conventional solvents nor in ILs, the former being only slightly more active. This may be ascribed, at least partially, to the fact that the diverse lengths of the alkyl side-chain of the ligands, being too far from the catalytically active metal centre, are unable to somehow diversify the outcome of catalytic runs. For the reactions performed in ILs, the following order of activity, BMIM-PF₆ > BMIM-OTf > BMIM-BF₄, observed in the oxidation of DBT and DMDBT and also detected during olefins oxidation, is in accordance with previous results from literature. Very interestingly, the system formed by complex **I** and BMIM-PF₆ used for the study of DBT oxidation with TBHP showed to be stable, retaining the activity of the catalyst caught inside the IL phase and so allowing its recyclability, without a relevant catalyst leaching, at least for five running cycles. Quantum-chemical calculations have shown that, in conventional solvents, the species, and hence the whole mechanism, might be different according to the diverse main oxidants used. The lower efficiency observed with H₂O₂ in chlorinated solvents, has been mainly ascribed to the water/solvent partition coefficient particularly low in the case of H₂O₂.

Finally, preliminary calculations carried out for roughly modelling what might happen when IL are used, suggest that the VO(Q^{Me})₂ initial adduct might undergo a partial or complete disruption essentially due to the vanadyl-IL anion interaction. This observation might qualitatively explain the substantially not so relevant efficiency observed in ILs, in comparison to conventional solvents, but it requires further investigations, at the moment rather difficult for the high complexity for the computational IL modelling.

CRediT authorship contribution statement

Patrizio Campitelli: Investigation, Formal analysis. **Massimiliano Aschi:** Investigation. **Corrado Di Nicola:** Formal analysis. **Fabio Marchetti:** Conceptualization, Writing - review & editing. **Riccardo Pettinari:** Validation. **Marcello Crucianelli:** Conceptualization, Writing - review & editing.

Declaration of Competing Interest

The authors declare that they have no known competing financial interests or personal relationships that could have appeared to influence the work reported in this paper.

Acknowledgment

The Universities of L'Aquila and Camerino are gratefully acknowledged for financial support. Authors thank Mr. Renato Di Bartolomeo (University of L'Aquila) for his help in the preparation of the graphics of the manuscript.

Appendix A. Supplementary data

Supplementary data associated with this article can be found, in the online version, at <https://doi.org/10.1016/j.apcata.2020.117622>.

References

- [1] G. Strukul, *Catalytic Oxidations with Hydrogen Peroxide As Oxidant*, Kluwer Academic Publishers, Dordrecht, 1992.
- [2] W. Adam, *Peroxide chemistry. Mechanistic and Preparative Aspects of Oxygen Transfer*, Wiley-VCH, Weinheim, 2000.
- [3] V. Conte, O. Bortolini, *Transition Metal Peroxides, Synthesis and Role in Oxidation Reactions*, Wiley Online Library, Weinheim, 2009.
- [4] W. Adam, W. Malisch, K.J. Roschmann, C.R. Saha-Möllner, W.A. Schenk, *J. Organomet. Chem.* 661 (2002) 3–16.
- [5] D.C. Crans, J.J. Smeee, E. Gaidamauskas, L. Yang, *Chem. Rev.* 104 (2004) 849–902.
- [6] D. Rehder, *Metallomics.* 7 (2015) 730–742.
- [7] J.C. Pessoa, S. Etcheverry, D. Gambino, *Coord. Chem. Rev.* 301 (2015) 24–48.
- [8] A. Butler, M.J. Clague, G.E. Meister, *Chem. Rev.* 94 (1994) 625–638.
- [9] K.A. Jørgensen, *Chem. Rev.* 89 (1989) 431–458.
- [10] F. Farzaneh, Z. Asgharpour, *Appl. Organomet. Chem.* 33 (2019) e4896.
- [11] R. Tan, C. Li, Z. Peng, D. Yin, D. Yin, *Catal. Commun.* 12 (2011) 1488–1491.
- [12] M.R. Maurya, M. Kumar, S.J.J. Titinchi, H.S. Abbo, S. Chand, *Catal. Letters* 86 (2003) 97–105.
- [13] S. Rezaei, A. Ghorbani-Choghamarani, R. Badri, A. Nikseresh, *Appl. Organomet. Chem.* 32 (2018) e3948.
- [14] H.P. Mungse, S. Verma, N. Kumar, B. Sain, O.P. Khatri, *J. Mater. Chem.* 22 (2012) 5427–5433.
- [15] M.R. Maurya, U. Kumar, I. Correia, P. Adão, J. Costa Pessoa, *Eur. J. Inorg. Chem.* 2008 (2008) 577–587.
- [16] J. Hartung, *Pure Appl. Chem.* 77 (2005) 1559–1574.
- [17] I. Lippold, J. Becher, D. Klemm, W. Plass, *J. Mol. Catal. A Chem.* 299 (2009) 12–17.
- [18] S. Parihar, R.N. Jadeja, V.K. Gupta, *RSC Adv.* 4 (2014) 10295–10302.
- [19] F. Marchetti, C. Pettinari, C. Di Nicola, A. Tombesi, R. Pettinari, *Coord. Chem. Rev.* 401 (2019) 213069.
- [20] F. Marchetti, R. Pettinari, C. Pettinari, *Coord. Chem. Rev.* 303 (2015) 1–31.
- [21] F. Marchetti, C. Pettinari, R. Pettinari, *Coord. Chem. Rev.* 249 (2005) 2909–2945.
- [22] V. Conte, B. Floris, *Inorganica Chim. Acta* 363 (2010) 1935–1946.
- [23] G. Silva, S. Voth, P. Szymanski, E.M. Prokopchuk, *Fuel Process. Technol.* 92 (2011) 1656–1661.
- [24] M. Sedighipour, A.H. Kianfar, W.A.K. Mahmood, M.H. Azarian, *Inorganica Chim. Acta* 457 (2017) 116–121.
- [25] G. Grivani, G. Bruno, H.A. Rudbari, A.D. Khalaji, P. Pourteimouri, *Inorg. Chem. Commun.* 18 (2012) 15–20.
- [26] A.C.V. Conte, P. Galloni, M. Centazzo, *Process for Desulphurisation of Fuels*, WO 2015/162162 AI, 2015.
- [27] A.S. Ogunlaja, W. Chidawanyika, E. Antunes, M.A. Fernandes, T. Nyokong, N. Torto, Z.R. Tshentu, *Dalton Trans.* 41 (2012) 13908–13918.
- [28] M.R. Maurya, A. Arya, A. Kumar, M.L. Kuznetsov, F. Avelilla, J. Costa Pessoa, *Inorg. Chem.* 49 (2010) 6586–6600.
- [29] H. Olivier-Bourbigou, L. Magna, D. Morvan, *Appl. Catal. A Gen.* 373 (2010) 1–56.
- [30] A. Mota, N. Butenko, J.P. Hallett, I. Correia, *Catal. Today* 196 (2012) 119–125.
- [31] S. Zhang, J. Sun, X. Zhang, J. Xin, Q. Miao, J. Wang, *Chem. Soc. Rev.* 43 (2014) 7838–7869.
- [32] M. Lombardo, C. Trombini, *ChemCatChem.* 2 (2010) 135–145.
- [33] F. Marchetti, C. Di Nicola, R. Pettinari, C. Pettinari, I. Aiello, M. La Deda, A. Candrea, S. Morelli, L. De Bartolo, A. Crispini, *Eur. J. Inorg. Chem.* (2019).
- [34] J. Palmucci, F. Marchetti, R. Pettinari, C. Pettinari, R. Scopelliti, T. Riedel, B. Therrien, A. Galindo, P.J. Dyson, *Inorg. Chem.* 55 (2016) 11770–11781.
- [35] C. Di Nicola, F. Marchetti, R. Pettinari, A. Tombesi, C. Pettinari, I. Grappasonni, P.J. Dyson, *S. Scuri, Materials (Basel).* 13 (2020) 526.
- [36] C. Pettinari, F. Marchetti, R. Pettinari, Y.A. Belousov, I.V. Taydakov, V.D. Krasnobrov, D.I. Petukhov, A.A. Drozdov, *Dalton Trans.* 44 (2015) 14887–14895, <https://doi.org/10.1039/c5dt01964h>.
- [37] F. Marchetti, C. Pettinari, C. Di Nicola, R. Pettinari, A. Crispini, M. Crucianelli, A. Di Giuseppe, *Appl. Catal. A Gen.* 378 (2010) 211–220.
- [38] A. Di Giuseppe, C. Di Nicola, R. Pettinari, I. Ferino, D. Meloni, M. Passacantando, M. Crucianelli, *Catal. Sci. Technol.* 3 (2013) 1972–1984.
- [39] M.M. Cecchini, F. De Angelis, C. Iacobucci, S. Reale, M. Crucianelli, *Appl. Catal. A Gen.* 517 (2016) 120–128.
- [40] R.R. Langeslay, D.M. Kaphan, C.L. Marshall, P.C. Stair, A.P. Sattelberger, M. Delferro, *Chem. Rev.* 119 (2018) 2128–2191.
- [41] J. Harvey, M. Aschi, H. Schwarz, W. Koch, *Theor. Chem. Acc.* 99 (1998) 95–99, <https://doi.org/10.1007/s002140050309>.
- [42] S. Miertuš, E. Scrocco, J. Tomasi, *Chem. Phys.* 55 (1981) 117–129.
- [43] M. Cossi, N. Rega, G. Scalmani, V. Barone, *J. Comput. Chem.* 24 (2003) 669–681.
- [44] T. Yanai, D.P. Tew, N.C. Handy, *Chem. Phys. Lett.* 393 (2004) 51–57.
- [45] P.J. Hay, W.R. Wadt, *J. Chem. Phys.* 82 (1985) 299–310, <https://doi.org/10.1063/1.448975>.
- [46] C. Chiappe, C.S. Pomelli, *Phys. Chem. Chem. Phys.* 15 (2013) 412–423.
- [47] M.R. Maurya, *Coord. Chem. Rev.* 237 (2003) 163–181.
- [48] J. Selbin, L.H. Holmes Jr., S.P. McGlynn, *J. Inorg. Nucl. Chem.* 25 (1963) 1359–1369.
- [49] C. Pettinari, F. Marchetti, A. Drozdov, *Compr. Coord. Chem. II.* (2003) 97–115.

- [50] J. Selbin, Chem. Rev. 65 (1965) 153–175.
- [51] S. Parihar, S. Pathan, R.N. Jadeja, A. Patel, V.K. Gupta, Inorg. Chem. 51 (2012) 1152–1161.
- [52] K. Kustin, D.L. Toppen, Inorg. Chem. 12 (1973) 1404–1407.
- [53] Y. Xiao, H. Huang, D. Yin, D. Guo, L. Mao, Z. Fu, Catal. Commun. 10 (2008) 29–32.
- [54] S. Vezzosi, A.G. Ferré, M. Crucianelli, C. Crestini, R. Saladino, J. Catal. 257 (2008) 262–269.
- [55] P. Adão, J. Costa Pessoa, R.T. Henriques, M.L. Kuznetsov, F. Avecilla, M.R. Maurya, U. Kumar, I. Correia, Inorg. Chem. 48 (2009) 3542–3561.
- [56] M. Aschi, M. Crucianelli, A. Di Giuseppe, C. Di Nicola, F. Marchetti, Catal. Today 192 (2012) 56–62.
- [57] R. Bikas, M. Ghorbanloo, S. Jafari, V. Eigner, M. Dusek, Inorganica Chim. Acta 453 (2016) 78–85.
- [58] A. Mota, J.P. Hallett, M.L. Kuznetsov, I. Correia, Phys. Chem. Chem. Phys. 13 (2011) 15094–15102.
- [59] S. Rayati, A. Ghaemi, N. Sadeghzadeh, Catal. Commun. 11 (2010) 792–796.
- [60] A.S. Ogunlaja, R.S. Walmsley, C. du Sautoy, N. Torto, Z.R. Tshentu, Energy Fuels 27 (2013) 7714–7723.
- [61] R. Saladino, G. Botta, M. Crucianelli, Advances in Nanotechnology Transition Metal Catalysts in Oxidative Desulfurization (ODS) Processes: Nanotechnology Applied to ODS Processing, Appl. Nanotechnol. to Desulfurization Process Pet. Eng., IGI Global (2016) 180–215.
- [62] M. Crucianelli, B.M. Bizzarri, R. Saladino, Catalysts 9 (2019) 984.
- [63] B. Rodríguez-Cabo, H. Rodríguez, E. Rodil, A. Arce, A. Soto, Fuel 117 (2014) 882–889.
- [64] C. Wang, Z. Chen, X. Yao, W. Jiang, M. Zhang, H. Li, H. Liu, W. Zhu, H. Li, RSC Adv. 7 (2017) 39383–39390.
- [65] S. Otsuki, T. Nonaka, N. Takashima, W. Qian, A. Ishihara, T. Imai, T. Kabe, Energy Fuels 14 (2000) 1232–1239.
- [66] J.M. Campos-Martin, M.C. Capel-Sanchez, J.L.G. Fierro, Green Chem. 6 (2004) 557–562.
- [67] L. Cedeño-Caero, H. Gomez-Bernal, A. Fraustro-Cuevas, H.D. Guerra-Gomez, R. Cuevas-Garcia, Catal. Today 133 (2008) 244–254.
- [68] J.W. Lee, J.Y. Shin, Y.S. Chun, H. Bin Jang, C.E. Song, S. Lee, Acc. Chem. Res. 43 (2010) 985–994.